https://doi.org/10.5194/egusphere-2025-3671
Preprint. Discussion started: 25 August 2025

Sinking particle fluxes and biological carbon pump efficiency in the Labrador Sea during a *Phaeocystis* bloom decline

Montserrat Roca-Martí[1,2], Madeline Healey[1], Colleen E. McBride[3], Rachel Sipler[3,4], Emmanuel Devred[5], Carolina Cisternas-Novoa[6], Elisa Romanelli[7], Kyoko Ohashi[1,8], Stephanie S. Kienast[1]

[1]Department of Oceanography, Dalhousie University, Halifax, NS, Canada
[2]Institut de Ciència i Tecnologia Ambientals (ICTA-UAB), Universitat Autònoma de Barcelona, Cerdanyola del Vallès, Spain
[3]Department of Ocean Sciences, Memorial University of Newfoundland, St. John's, NL, Canada
[4]Bigelow Laboratory for Ocean Sciences, East Boothbay, ME, USA
[5]Fisheries and Oceans Canada, Bedford Institute of Oceanography, Dartmouth, NS, Canada
[6]Ocean Sciences Centre, Memorial University of Newfoundland, St. John's, NL, Canada
[7]Institute of Environmental Engineering, Department of Civil, Environmental and Geomatic Engineering, ETH Zurich, Zurich, Switzerland
[8]Fisheries and Oceans Canada, Institute of Ocean Sciences, Sidney, BC, Canada

Correspondence to: Montserrat Roca-Martí (montserrat.roca.marti@uab.cat)

Abstract. The Labrador Sea is a key region for carbon dioxide uptake characterized by deep mixing during winter that supplies nutrients to the upper water column and fuels extensive phytoplankton blooms in spring. Yet, the efficiency by which organic carbon is exported from surface waters during these blooms, as well as their contribution to carbon sequestration, remain poorly constrained. Here, we present an unprecedented number of measurements of sinking export fluxes (particulate organic carbon, POC; and biogenic silica, bSi) collected in the central Labrador Sea during a 2-week-long process study that observed the decline of a historically large *Phaeocystis* bloom in spring 2022. This *Phaeocystis* bloom was unusually large and highly productive, extending over more than half of the Labrador Sea for 6 weeks. During the late stages of the bloom, we found that POC fluxes from the base of the euphotic zone to 500 m were variable but overall moderate to high (average of 8 ± 5 mmol C m^{-2} d^{-1}). Nevertheless, evidence of shallow POC flux remineralization combined with the fact that POC fluxes in the bloom were not higher than in a region sampled outside of the bloom (average of 13 ± 3 mmol C m^{-2} d^{-1}) suggested a limited role of *Phaeocystis* in carbon export. Large (>51 μm) particles collected using large volume pumps presented relatively low bSi/POC ratios and, therefore, diatoms did not appear to have an important ballasting role of *Phaeocystis*-derived material. Using in situ net primary production (NPP) rates, we determined that 2 weeks after the peak of the bloom, the total amount of NPP that reached 100 m below the euphotic zone was only 6%. However, 3 weeks after the peak of the bloom, the value had increased to 29%. The observed change was driven primarily by a decline in NPP over the sampling period, as POC fluxes remained relatively constant. Using satellite-derived NPP from the peak of the bloom until its end, we obtained an overall biological carbon pump (BCP) efficiency of 6% placing this *Phaeocystis* bloom as a low BCP efficiency system. We stress the importance of long-term observations of both NPP and POC export for estimating meaningful BCP efficiencies. The results presented in this study provide a foundation for comparisons with other datasets collected during this ship-based process study and autonomous platforms present in the area during and beyond this study. These future efforts will provide the opportunity to increase the observational period and further elucidate the mechanisms leading to the low BCP efficiency found during the decline of this *Phaeocystis* bloom in the Labrador Sea.

https://doi.org/10.5194/egusphere-2025-3671
Preprint. Discussion started: 25 August 2025

1. Introduction

The biological carbon pump (BCP) encapsulates a set of processes that remove carbon dioxide (CO_2) from the atmosphere and sequester it in the deep ocean (Passow and Weber, 2025; Volk and Hoffert, 1985). In the surface ocean, phytoplankton produce organic matter via photosynthesis, and a fraction of this organic matter is subsequently transferred to depth through sinking and other processes. Most of this material is decomposed and respired in the ocean interior, where CO_2 remains stored for several centuries or longer until it is brought back to the surface ocean by physical transport. A very small fraction of exported carbon is buried in seafloor sediments and thus removed from the atmosphere on geological timescales. While it is well understood that the BCP plays a large role in climate regulation, there is low confidence in the magnitude and even the sign of predicted near-future changes in carbon export fluxes and how these will in turn affect atmospheric CO_2 levels (Henson et al., 2022). Better quantification of particulate matter fluxes in the ocean is thus urgently needed.

Indeed, the various processes transforming and redistributing carbon between the surface and the deep ocean remain poorly quantified. Assessments of carbon budgets below the euphotic zone typically have found that organic carbon sources and sinks are not balanced (Baltar et al., 2009; Boyd et al., 1999; Burd et al., 2010; Reinthaler et al., 2006; Steinberg et al., 2008). This mismatch has been attributed to methodological constraints, the choice of parameters used to estimate budget terms, the exclusion of important midwater processes, and the spatial and temporal scales over which measurements are integrated (Baumas et al., 2023; Giering et al., 2014; Stephens and Roca-Martí et al., 2025).

Major uncertainties in the magnitude of biologically driven carbon ocean uptake and storage also lie in our fragmented understanding of the different pathways by which the BCP exports particulate and dissolved organic carbon (POC and DOC, respectively) from surface waters to the deep ocean. Advances in remote sensing, in situ imagery, and the development of autonomous platforms (BGC-Argo floats and gliders) over the last 2 decades have revealed that the BCP includes six major pathways for exporting organic carbon from the surface ocean to the deep ocean: gravitational export (sinking), three pumps driven by physical processes (mixed layer, eddy subduction and large-scale subduction), and two pumps driven by vertical migrations of zooplankton and larger animals (Boyd et al., 2019; Claustre et al., 2021). Process studies and long-term observations of the BCP, combining multiple approaches both ship- and autonomous-based, have been shown to be crucial for better constraining ocean carbon budgets (Stephens and Roca-Martí et al., 2025).

The North Atlantic is responsible for a significant fraction of the global carbon export (~15%), driven by a complex set of BCP processes (Sanders et al., 2014). The subpolar North Atlantic, specifically the Labrador Sea, is an important region for CO_2 uptake (Arruda et al., 2024) characterized by deep vertical mixing during winter that supplies nutrients to the upper water column and fuels extensive phytoplankton blooms in spring after the water column has stratified (Tesdal et al., 2022). Yet, the efficiency by which organic carbon is exported from surface waters during these blooms as well as their contribution to carbon sequestration remain poorly constrained, partly because of the complex physical processes in the region (Baker et al., 2022) and the very limited POC flux observations made so far (e.g., Lemaitre et al., 2018). In addition, impacts of global warming in the physical conditions of the Labrador Sea have already been reported, including freshening and weaker winter convection

https://doi.org/10.5194/egusphere-2025-3671
Preprint. Discussion started: 25 August 2025

(Yashayaev, 2024), which add uncertainty to the future state of the BCP and its downstream effects on climate and marine ecosystems.

The phytoplankton assemblages in the Labrador Sea are typically dominated by diatoms, *Phaeocystis* spp. or mixed populations (Devred et al., 2024). Observations of *Phaeocystis* blooms were previously restricted to shelf and slope regimes, but unprecedented large *Phaeocystis* blooms have been reported in the Labrador basin in recent years (in 2015 and 2022; Devred et al., 2025). Here, we present measurements of net primary production (NPP) and sinking export fluxes (POC and biogenic silica, bSi) in the central Labrador Sea during the decline of a historically large *Phaeocystis* bloom in spring 2022. The novelty of our ship-based process study (Biological Carbon Export in the Labrador Sea, BELAS-1) lies in the high temporal resolution of in situ measurements collected over 2 weeks which shed light on the efficiency of the gravitational sinking pump of *Phaeocystis* blooms.

2. Methods

Samples were collected in the Labrador Sea from 19 May to 2 June 2022 during the BELAS-1 expedition (CE22009, RV *Celtic Explorer*). Three regions were targeted (Fig. 1): a grid of nine stations (hereafter "Eastern Grid", ~1075 km^2), where an extensive *Phaeocystis pouchetii* bloom was in decline (Devred et al., 2025; Bertrand et al., in prep); two stations located outside of the major *Phaeocystis* bloom to the southwest of the Eastern Grid (hereafter "Central"); and one station located in the bloom area between the Eastern Grid and the central stations which was sampled on two consecutive days (hereafter "Station 28-1" and "Station 28-2"). In the Eastern Grid, six stations were sampled from 20 May to 25 May (hereafter "East 1") before Station 28 and the central stations were occupied, while three stations were sampled after a major storm (Bertrand et al., in prep) at the end of the expedition from 30 May to 2 June (hereafter "East 2"). East 1 was characterized by higher *Phaeocystis* biomass levels and primary production rates compared to East 2, which represented post-bloom conditions (Fig. 2 and 3).

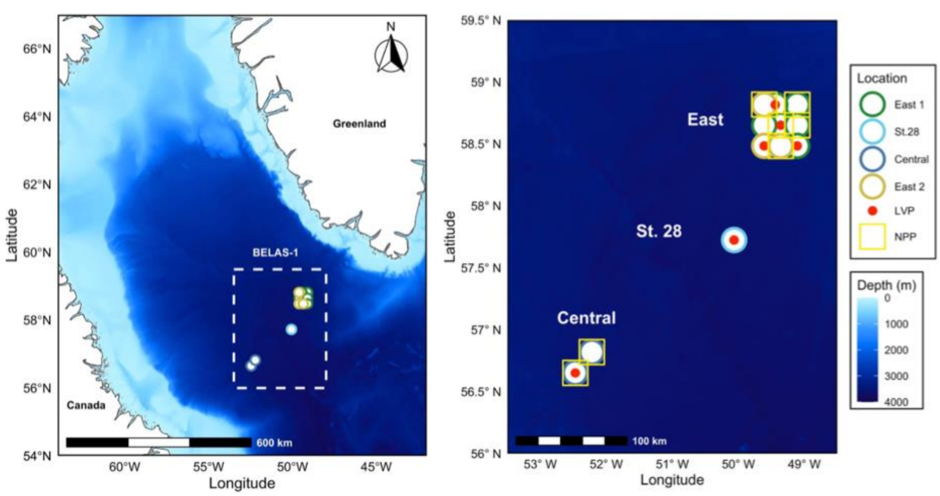

https://doi.org/10.5194/egusphere-2025-3671
Preprint. Discussion started: 25 August 2025

Figure 1. Map of the stations sampled during the BELAS-1 expedition (CE22009, RV *Celtic Explorer*) in different regions: the Eastern Grid or "East" (East 1: 20 May to 25 May; East 2: 30 May to 2 June), Station 28 (St. 28), and "Central". All stations were sampled for total ^{234}Th in seawater. Red dots denote stations where in situ large volume pumps (LVP) were deployed. Yellow squares denote stations sampled for net primary production (NPP).

The mixed layer depth (MLD), defined as the depth where potential density exceeds the density at 10 m depth by 0.03 kg m^{-3} (de Boyer Montégut et al., 2004), ranged from 22 to 66 m. Stratification, defined as the squared buoyancy frequency, ranged from 5 to 88 m and was on average 20% deeper than the MLD. The base of the primary production zone (PPZ), defined as the depth at which fluorescence was 10% of its maximal value (Owens et al., 2015), ranged from 79 to 176 m and was used to operationally define the base of the euphotic zone. Fluorescence was obtained from an optical package mounted on the conductivity-temperature-depth (CTD) rosette system. The CTD was not equipped with a photosynthetic active radiation (PAR) sensor during the BELAS-1 expedition.

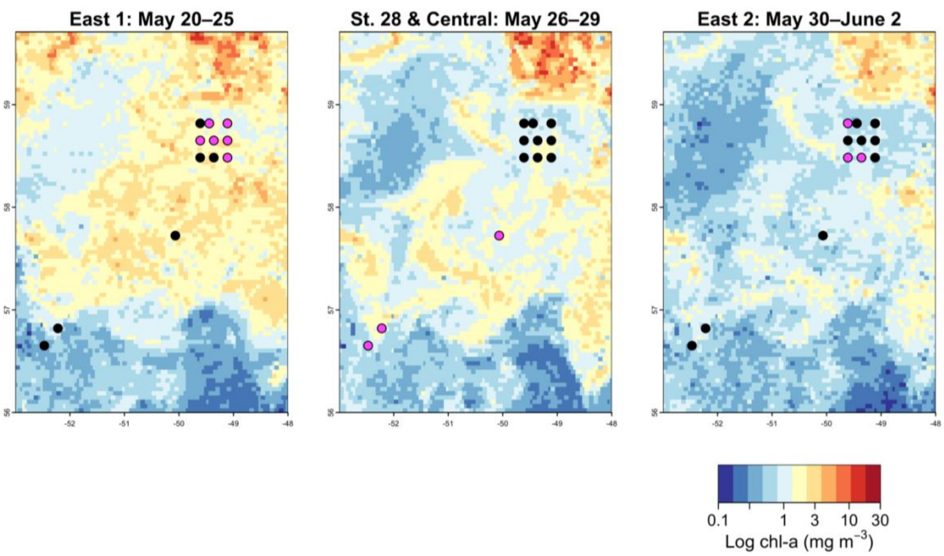

Figure 2. Satellite-derived chlorophyll-a (chl-a) concentrations (Devred et al., 2025) at the time of sampling of East 1 stations (left panel), Station 28 and central stations (middle panel), and East 2 stations (right panel).

2.1. Net primary production

Water was collected from six depths using a CTD-rosette fitted with 10 L Niskin bottles. While collections were dispersed throughout the upper 200 m of the water column, some sampling depths were selected based on key hydrographic features, including the surface and chlorophyll-a (chl-a) maximum. Water was transferred from the Niskin to the incubation bottles using acid-rinsed (10% HCl followed by a minimum of four rinses with type 1 water) silicone tubing fitted with 150 µm Nitex mesh and covered in electrical tape to exclude light from samples collected at depth. Incubations were performed in triplicate in acid-washed 1 L incubation bottles filled to the bottle neck (approximate volume of 1.2 L). Bottles were amended with $H^{13}CO_3^-$ (99%; Cambridge Isotope Laboratories) at an approximate addition of 330 µmol C L^{-1}. For stable isotope tracer studies, we aim for target additions of 10%, and the average atom percent enrichment for the current study was 13.8 ± 0.5%.

https://doi.org/10.5194/egusphere-2025-3671
Preprint. Discussion started: 25 August 2025

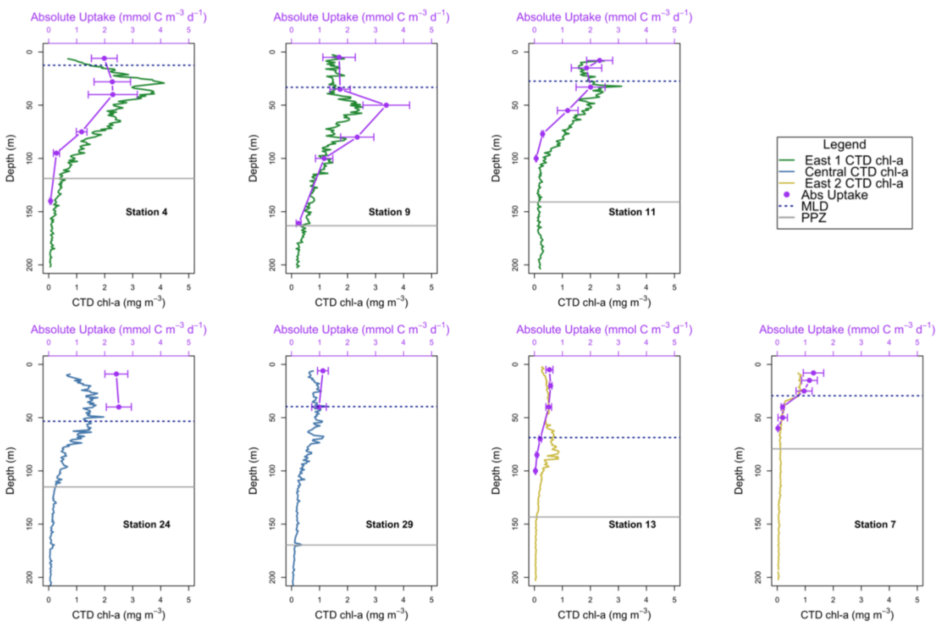

Figure 3. Profiles of chlorophyll-a from the CTD (CTD chl-a) and net primary production (NPP, absolute uptake) in the upper 200 m of the water column in East 1 (green), Central (dark blue) and East 2 (yellow) stations. The base of the primary production zone (PPZ, Owens et al., 2015) shown with a grey solid line is used to operationally define the base of the euphotic zone. The base of the mixed layer (MLD) is shown with a blue dashed line.

Once the isotope was added, bottles were placed in flow-through deck incubators for 24 h with natural daylight. Incubators were covered at night to prevent the unintended impacts of deck lighting. The incubation bottles were covered with screen bags of varying thicknesses to mimic the light availability at the depth where they were collected. For deep samples, bottles were covered with foil and then multiple layers of electrical tape to eliminate light intrusion. Temperature and light in the incubators were monitored using HOBO TidbiT v2 water temperature data loggers (Onset Computer Corporation).

The experiments were terminated by filtration onto pre-combusted (450°C for 4 h) GF-75 filters with a nominal pore size of 0.3 µm. Filters were placed into 2 mL cryovials and frozen at -20°C until analysis at Bigelow Laboratory for Ocean Sciences using a CosTech ECS 4010/Thermo DELTA V Advantage Isotope Ratio Mass Spectrometer by the Bigelow Analytical Services. Absolute carbon uptake rates were calculated according to Hama et al. (1983) using the following equation:

$$\rho = \frac{PC\ at\%xs}{DIC\ at\%xs \times Time} \times [PC], \tag{1}$$

where ρ is the absolute uptake rate (mmol C m^{-3} d^{-1}) and *at%xs* refers to the excess percentage of ^{13}C atoms in relation to the natural abundance of either particulate carbon (PC) or dissolved inorganic carbon (DIC). Ambient HCO_3^- concentrations were estimated based on the salinity of each sample (Parsons et al., 1984).

https://doi.org/10.5194/egusphere-2025-3671
Preprint. Discussion started: 25 August 2025

Depth-integrated NPP was calculated for stations located in the Eastern Grid using a midpoint box integration up to the base of the PPZ that incorporated both measured absolute uptake rates and chl-a concentrations. Due to a limited number of sampling depths, NPP could not be integrated at the central stations. A trapezoidal integration is typically recommended for calculating depth-integrated NPP from in situ rate measurements (Knap et al., 1996), but this method can have difficulties when there are variances in sampling depth across and within stations, as was the case in the BELAS-1 expedition. Despite these variances, the midpoint box and trapezoidal integrations only differed by a maximum of 2.5% across Eastern Grid stations. However, the trapezoidal integration led to increased differences in depth-integrated NPP when incorporating chl-a concentrations (up to 18%) compared to the midpoint box integration. Therefore, the more conservative midpoint box approach was taken. Chl-a concentrations were used to calculate depth-integrated NPP to determine if a relationship between absolute uptake rates and chl-a could be used to model depth-integrated NPP at the central stations. However, no clear relationship was determined. Fluorometer profiles from the CTD were adjusted using a regression based on chl-a concentrations measured by high-performance liquid chromatography (HPLC) but were not corrected for non-photochemical quenching (NPQ) due to the presence of a subsurface chl-a maximum (Bertrand et al., in prep). Chl-a concentrations near the surface should, therefore, be considered slightly underestimated, but this is likely to have little to no impact on the rate when integrated over the water column. The difference in depth-integrated NPP with and without the inclusion of chl-a concentrations ranged from 0.1% (Station 7) to 11% (Station 4). In cases where the base of the PPZ exceeded the deepest sampling depth, the absolute uptake rate from the deepest sampling depth was used for any depths up to and including the base of the PPZ.

2.2. Total ^{234}Th and ^{238}U in seawater

Water column samples were taken in the upper 500 m of all stations (n = 12, Fig. 1, 4) using a CTD-rosette at 15 discrete depths. Unfiltered seawater samples (2 L) were processed on board and analyzed for the activity of total (dissolved + particulate) ^{234}Th following the method described in Clevenger et al. (2021). Samples were immediately acidified after collection and spiked with a yield monitor (^{230}Th, 25 disintegrations per minute, dpm, per sample). After a minimum 6 h equilibration time, sample pH was increased to ~8.5 using ammonium hydroxide, and reagents were added to form a manganese oxide precipitate for scavenging of Th. Samples were allowed to stand for at least 8 h, filtered onto 25-mm diameter quartz microfiber filters (QMA), dried and mounted for beta counting. Samples were counted using three low-level Risø beta multicounters (5 detectors each) until the error was typically <3%. Beta counters were calibrated using two sets of five deep samples (1500 m) from two stations. At least 5 months after collection (>6 ^{234}Th half-lives, where the half-life = 24.1 d), samples were recounted at Dalhousie University to determine the non-^{234}Th beta activity stemming from other radionuclides included in the precipitate, which was subtracted from the first count. The net counting rate was corrected for ^{234}Th decay and ingrowth from ^{238}U, counting efficiency and chemical recovery. The chemical recovery of ^{230}Th was determined by using a Thermo Scientific iCAP quadrupole inductively coupled plasma mass spectrometer (ICP-MS) following the procedure detailed in Clevenger et al. (2021). Recoveries averaged 83 ± 10% (n = 218). The uranium-238 (^{238}U) activity was derived from salinity (Owens et al., 2011).

https://doi.org/10.5194/egusphere-2025-3671
Preprint. Discussion started: 25 August 2025

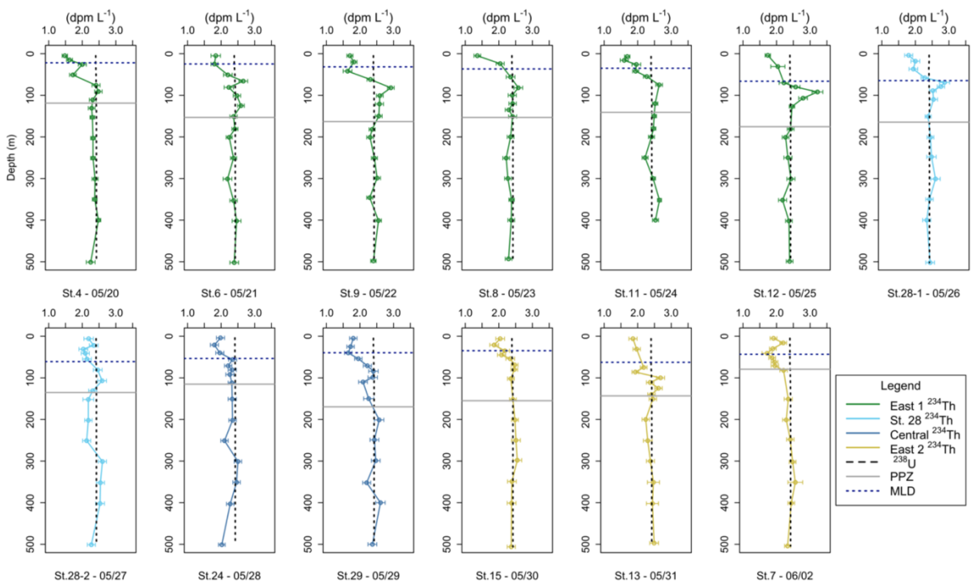

Figure 4. Profiles of total ^{234}Th and ^{238}U in the upper 500 m of the water column in East 1 stations (green), Station 28 (light blue), central stations (dark blue) and East 2 stations (yellow). The base of the primary production zone (PPZ) is shown with a grey solid line and the base of the mixed layer (MLD) is shown with a blue dashed line.

2.3. Particles collected using large volume pumps and marine snow catchers

Size-fractionated particles were collected using battery-powered in situ large volume pumps (McLane Research Laboratories, Inc.) equipped with a three-tier 142-mm diameter filter holder (MULVFS style; Bishop et al., 2012; Lam et al., 2015). Five pumps were deployed at depths between 40 and 490 m at six stations (Fig. 1, 5). The pump deployment depths were chosen after examining the fluorescence profile from a CTD cast conducted shortly prior to the pump deployment. One pump was placed close to the base of the PPZ and another pump at 100 m below the PPZ base. Pumps were programmed to sample for 2.5 to 3.0 h at a starting flow rate of 6 L min^{-1} and pumped an average of 460 L each. During each pump deployment, pressure sensors (RBR duet 3) were attached to selected pumps to confirm deployment depths.

The filter holders contained three filters: two Nitex screens (335 and 51 µm nominal pore size, acid-leached prior to the cruise) above a pre-combusted QMA filter (~1 µm nominal pore size, Graff et al., 2023) for size fractionation (1–51, 51–335 and >335 µm). A total of 28 samples were collected for each size fraction. Size-fractionated particles were analyzed for ^{234}Th, particulate organic carbon (POC), and biogenic silica (bSi, only from Nitex screens, i.e., 51–335 and >335 µm size fractions). In every cast, an additional filter holder was mounted on the deepest pump to obtain a seawater process blank ("dipped blank" filters, Lam et al., 2015). Immediately after recovering the pumps, residual water from each filter holder was removed by vacuum to avoid particle loss.

https://doi.org/10.5194/egusphere-2025-3671
Preprint. Discussion started: 25 August 2025

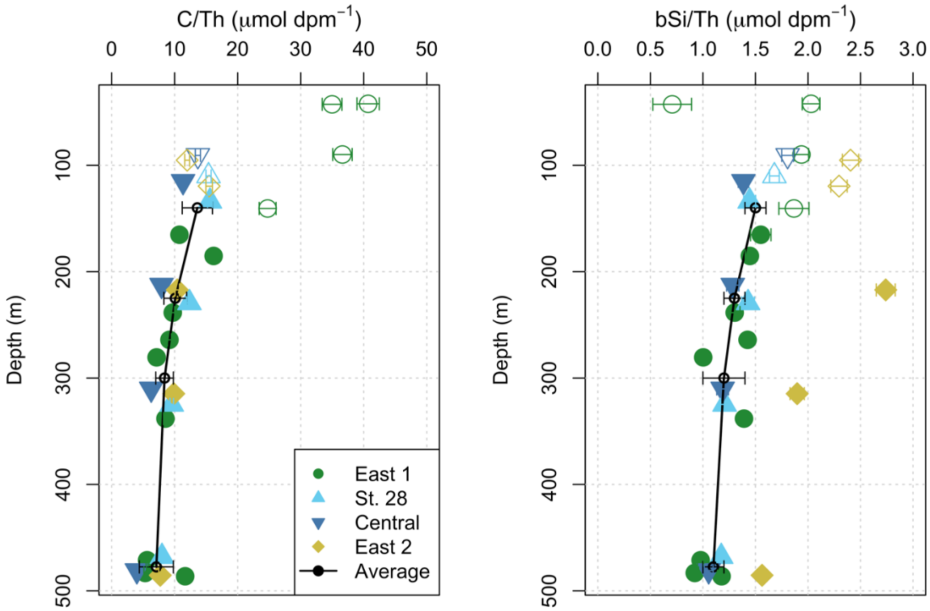

Figure 5. Profiles of POC/^{234}Th (C/Th) and bSi/^{234}Th (bSi/Th) ratios in >51 µm particles across regions. Black symbols denote average C/Th ratios (all stations) and average bSi/Th ratios (all stations except East 2) for the following depth horizons: 115–185, 210–240, 260–340, 465–490 m. Empty symbols denote samples collected within the primary production zone. POC = particulate organic carbon, bSi = biogenic silica.

Zooplankton that were not part of the passive sinking flux ("swimmers") and were visible to the naked eye were carefully handpicked from the Nitex screens using forceps and discarded. Particles were gently rinsed off the Nitex screens onto 25-mm-diameter silver (Ag) filters (1.2 µm nominal pore size) using pre-filtered seawater. QMA filters were subsampled for ^{234}Th and POC using a circular punch tool. Ag and QMA filters were dried, beta counted at sea for ^{234}Th activities and recounted >5 months later at Dalhousie University. After final counting, Ag filters were split into halves by weight and analyzed for POC and bSi. POC was analyzed using high-temperature combustion (Costech Instruments Elemental Combustion System 4010) after acid fumigation. bSi was analyzed following the NaOH digestion method (40 min at 95ºC) using a UV-Visible Spectrophotometer (Genesys 10S, Thermo Scientific) as in Roca-Martí et al. (2021).

The average of all dipped blanks was subtracted from total ^{234}Th, POC, and bSi measurements. Dipped blanks contributed on average <3% to the total ^{234}Th measured on the filters, <7% to total bSi, and <14% to total POC (Table S1 in the Supplement). All concentrations were above the limit of detection (3 x standard deviation of the dipped blanks, Lam et al., 2018). Analysis of triplicate punches from four QMA filters representing depths from 100 to 500 m yielded a relative standard deviation for POC of 1–4%, indicating a relatively homogeneous particle distribution across the filters (Maiti et al., 2012). POC and bSi data have average uncertainties of 3% and 6%, respectively, resulting from the dipped blank correction. Particulate ^{234}Th have average uncertainties of 5% resulting from counting and the dipped blank correction.

https://doi.org/10.5194/egusphere-2025-3671
Preprint. Discussion started: 25 August 2025

At Station 12 in East 1, particles were also collected using marine snow catchers (MSCs, total volume of ~100 L). Three MSCs were deployed approximately 3.5 h prior to the large volume pump deployments at similar depths (165, 265, and 485 m; ± 5 m). After a 2 h settling period, subsamples were taken from each MSC: on average, 2.1 L (of 5.0 L) from the base compartment and 1.4 L (of 2.6 L) from the tray (located at the bottom of the base) were filtered through 25-mm-diameter Ag filters (0.45 µm nominal pore size) for the determination of ^{234}Th and POC in slow- and fast-sinking particles. Blank corrections were applied by subtracting the average of two filter blanks from total ^{234}Th and POC measurements, and the slow- and fast-sinking particle fractions were subsequently combined. Average uncertainties were 1% for POC and 17% for particulate ^{234}Th, resulting from the blank correction (POC and ^{234}Th) and counting (^{234}Th). The sample from 165 m was excluded from analysis due to a low signal-to-noise ratio in the ^{234}Th measurements. Further details on MSC deployments and sample processing are available in Romanelli et al. (2023) and Cisternas-Novoa et al. (in prep).

2.4. ^{234}Th, POC and bSi export fluxes

Export fluxes of ^{234}Th were calculated for each water column profile by integrating the disequilibrium between ^{234}Th and ^{238}U from the surface to each sampled depth over the upper 500 m of the water column. This model implies steady-state (SS) conditions and neglects physical transport (Roca-Martí and Puigcorbé, 2024; Savoye et al., 2006). We discuss the validity of this SS approach in Sect. 2.5.

To estimate POC and bSi export fluxes, steady-state ^{234}Th fluxes were multiplied with POC/^{234}Th (C/Th) and bSi/^{234}Th (bSi/Th) ratios measured in >51 µm particles (i.e., combining the 51–335 and >335 µm size fractions) collected using large volume pumps. Using the >51 µm fraction for the calculation of fluxes is consistent with the majority of ^{234}Th studies (Puigcorbé et al., 2020). Furthermore, this choice is directly supported here by comparing C/Th ratios measured at Station 12 in size-fractionated particles with those measured in sinking particles collected using MSCs (Fig. S1 in the Supplement). Sinking particles from MSCs show C/Th ratios similar to all pump size fractions that are greater than 51 µm (i.e., 51–335 µm, >335 µm, and >51 µm; Fig. S1 in the Supplement). On the contrary, C/Th ratios from MSCs are clearly higher than C/Th ratios in pump samples that include particles smaller than 51 µm (i.e., the 1–51 µm and >1 µm fractions).

Based on the samples collected at five depths across six individual stations, we derived average C/Th and bSi/Th ratios (± standard deviation) for several depth horizons below the PPZ base (115–185, 210–240, 260–340, 465–490 m; Fig. 5). Ratios at depths not sampled by pump deployments were interpolated linearly between the mid-points of each depth horizon. For POC, all pump casts were combined to determine cruise-average C/Th ratios because no significant differences were found between East 1, Station 28, Central, and East 2 (one-way ANOVA, $p > 0.05$). For bSi, pump casts from East 1, Station 28, and Central were combined (one-way ANOVA, $p > 0.05$) to determine average bSi/Th ratios and estimate bSi fluxes from 20 May to 29 May. bSi/Th ratios in East 2 were used to estimate bSi fluxes from 30 May to 2 June given the higher bSi/Th ratios measured in East 2 (Kruskal-Wallis, $p < 0.01$).

https://doi.org/10.5194/egusphere-2025-3671
Preprint. Discussion started: 25 August 2025

2.5. Testing the assumptions of our export model

2.5.1. How valid is the steady state assumption?

The validity of the steady state (SS) assumption during a phytoplankton bloom depends on when the sampling occurs with respect to the bloom peak and the duration of the bloom (Ceballos-Romero et al., 2018). Following the approach by Ceballos-Romero et al. (2018), satellite-derived chl-a concentrations suggest that the peak of maximum production in the Eastern Grid area occurred on 11 May, i.e., 9–22 d before our sampling period (20 May–2 June). Chl-a decreased quite rapidly with time after the peak (Fig. S2 in the Supplement), similar to a hypothetical bloom scenario considered in Ceballos-Romero et al. (2018) (their Fig. 1b). In such conditions, these authors found that the ^{234}Th SS model provides accurate flux estimates during a ~1 week-long sampling period, referred to as "window of success", which commences 10 d after the peak of the bloom. Comparing the sampling dates and bloom timing of the present study with the findings from Ceballos-Romero et al. (2018) suggests that most of our sampling in East 1 happened within the window of success (21 May–27 May, Fig. S2 in the Supplement), supporting the validity of the SS assumption. Sampling in East 2 occurred 3 to 6 d after the window of success, and therefore, fluxes at the end of the sampling period might represent high end-member estimates (Ceballos-Romero et al., 2018).

In addition, the sampling strategy of the BELAS-1 expedition was incompatible with a non-steady state (NSS) model given that: 1) the sampling period was relatively short (6 d in East 1 and 4 d in East 2) relative to the 2–3 weeks recommended by Ceballos-Romero et al. (2018) to capture changes, if any, in ^{234}Th activities vs. time and apply a NSS approach; and 2) in order to obtain accurate flux estimates with a NSS model, a Lagrangian sampling strategy that tracks the same water mass must be followed (Resplandy et al., 2012; Savoye et al., 2006), which was not possible during this expedition. Indeed, changes in upper water column properties occurred between the sampling of East 1 and East 2 due to a storm (Bertrand et al., in prep), indicating that different water masses might have been sampled. Further, in the Eastern Grid, where we have the highest density of measurements, we did not observe significant changes in ^{234}Th inventories in the upper 150 m over time (Fig. S3a in the Supplement). Thus, we consider that the SS model gives the best estimate of ^{234}Th export in this study.

2.5.2. Evaluating the effect of physical transport

Vertical Transport: The central Labrador Sea in 2022 experienced moderately deep convection reaching 1600 m (Yashayaev, 2024) followed by water column stratification and bloom development in early April. Winter mixing would homogenize vertical ^{234}Th gradients in the water column. However, sampling during BELAS-1 occurred at least 50 d after convection ended, a time interval that exceeds the half-life of ^{234}Th and its mean life (1/decay constant = 35 d). Therefore, we are confident that vertical advection associated with winter mixing did not influence the estimates presented in this study. The potential contribution of vertical diffusion was estimated using vertical diffusivity estimates from a hindcast simulation using the model of Ohashi et al. (2024) in the Eastern Grid at the time of the cruise. Vertical diffusivity decreased with depth from 10^{-4}–10^{-2} m^2 s^{-1} at the surface to 10^{-6} m^2 s^{-1} below 80 m. We estimate that vertical diffusion changed ^{234}Th fluxes at the base of the PPZ by <10 dpm m^{-2} d^{-1} only, given the small gradients in ^{234}Th activities observed across the base of the PPZ at each station (Fig. 4). Therefore, the influence of vertical transport on ^{234}Th export flux estimates must have been negligible.

https://doi.org/10.5194/egusphere-2025-3671
Preprint. Discussion started: 25 August 2025

Horizontal Transport: Horizontal advection in the Eastern Grid, derived from the hindcast simulation of the cruise period, had mean velocities of 2.8 km d^{-1} over the top 150 m in a mostly southeastward direction. The observed ^{234}Th activities show relatively large variability between profiles in the Eastern Grid (Fig. S4 in the Supplement), however, there are no consistent spatial trends in ^{234}Th inventories (Fig. S3b in the Supplement). We attribute the variability in ^{234}Th between profiles to small-scale spatial variations or patchiness rather than horizontal transport.

3. Results

Table 1 presents a summary of the integrated NPP rates down to the base of the PPZ, together with the sinking fluxes (POC, bSi) measured at different depths in the upper 500 m across all the stations sampled during BELAS-1.

3.1. NPP rates

The average NPP at the surface and chl-a maximum depths was higher in East 1 (2.01 and 2.56 mmol C m^{-3} d^{-1}) compared to Central (1.79 and 1.74 mmol C m^{-3} d^{-1}) and East 2 (0.92 and 0.75 mmol C m^{-3} d^{-1}), which correlates with decreasing chl-a concentrations over the sampling period (Fig. 3). Surface NPP was highest at Station 11 (2.36 ± 0.47 mmol C m^{-3} d^{-1}) while NPP at the chl-a maximum peaked at Station 9 (3.38 ± 0.83 mmol C m^{-3} d^{-1}). Station 13 had the lowest surface and chl-a maximum NPP, 0.54 ± 0.13 mmol C m^{-3} d^{-1} and 0.52 ± 0.10 mmol C m^{-3} d^{-1}, respectively. Depth-integrated NPP was highest during East 1, peaking at Station 9 with a value of 252 ± 6 mmol C m^{-2} d^{-1} (Table 1). Between sampling for East 1 and East 2, depth-integrated NPP decreased notably as the bloom declined and transitioned into post-bloom conditions, reaching a minimum of 39 ± 1 mmol C m^{-2} d^{-1} at Station 13 (Table 1).

Table 1. Integrated net primary production (NPP) down to the base of the primary production zone (PPZ), and particulate organic carbon (POC) and biogenic silica (bSi) fluxes at different depths across all stations.

Region	Station ID	Lat (ºN)	Long (ºE)	Sampling date (2022)	Base of PPZ (m)	Integrated NPP (mmol C m^{-2} d^{-1})	POC flux at PPZ base (mmol C m^{-2} d^{-1})	bSi flux at PPZ base (mmol Si m^{-2} d^{-1})	POC flux at PPZ base + 100 m (mmol C m^{-2} d^{-1})	bSi flux at PPZ base + 100 m (mmol Si m^{-2} d^{-1})	POC flux at 500 m (mmol C m^{-2} d^{-1})	bSi flux at 500 m (mmol Si m^{-2} d^{-1})
East 1	4	58.82	-49.11	20-May	119	188 ± 6	16.3 ± 4.0	1.8 ± 0.2	15.6 ± 3.5	2.1 ± 0.3	13.9 ± 6.1	2.1 ± 0.5
	6	58.82	-49.44	21-May	153	–	8.1 ± 3.1	0.9 ± 0.3	8.0 ± 2.7	1.1 ± 0.3	8.9 ± 5.0	1.3 ± 0.6
	9	58.65	-49.36	22-May	163	252 ± 6	6.2 ± 2.9	0.7 ± 0.3	5.2 ± 2.3	0.8 ± 0.3	3.0 ± 3.2	0.5 ± 0.4
	8	58.65	-49.61	23-May	153	–	9.3 ± 3.4	1.0 ± 0.3	9.1 ± 3.1	1.2 ± 0.4	11.8 ± 5.5	1.8 ± 0.5
	11	58.65	-49.11	24-May	141	125 ± 4	7.4 ± 2.7	0.8 ± 0.2	5.5 ± 2.3	0.7 ± 0.3	–	–
	12	58.48	-49.11	25-May	176	–	2.9 ± 3.8	0.3 ± 0.4	4.1 ± 3.1	0.6 ± 0.4	7.0 ± 4.6	1.1 ± 0.6
St. 28	28-1	57.72	-50.07	26-May	165	–	4.7 ± 3.0	0.5 ± 0.3	2.1 ± 2.5	0.3 ± 0.4	0.8 ± 3.7	0.1 ± 0.6
	28-2	57.72	-50.07	27-May	135	–	5.1 ± 2.9	0.5 ± 0.3	10.5 ± 3.6	1.4 ± 0.4	6.7 ± 4.6	1.0 ± 0.6
Central	24	56.65	-52.47	28-May	115	–	12.6 ± 3.3	1.4 ± 0.2	12.0 ± 3.4	1.6 ± 0.4	17.0 ± 7.4	2.6 ± 0.6
	29	56.82	-52.22	29-May	170	–	22.1 ± 5.8	2.4 ± 0.4	12.1 ± 3.7	1.8 ± 0.5	9.4 ± 5.5	1.4 ± 0.6
East 2	15	58.48	-49.61	30-May	155	–	7.2 ± 3.0	1.3 ± 0.4	3.4 ± 2.7	0.9 ± 0.7	2.7 ± 4.0	0.6 ± 0.8
	13	58.48	-49.36	31-May	143	39 ± 1	12.0 ± 3.6	2.1 ± 0.5	11.5 ± 3.3	3.0 ± 0.7	8.1 ± 5.3	1.8 ± 1.0
	7	58.82	-49.61	02-Jun	79	43 ± 2	13.9 ± 3.2	2.4 ± 0.2	18.7 ± 5.4	3.3 ± 0.7	9.9 ± 5.6	2.2 ± 0.9

https://doi.org/10.5194/egusphere-2025-3671
Preprint. Discussion started: 25 August 2025

3.2. ^{234}Th/^{238}U profiles and ^{234}Th fluxes

In the upper water column, ^{234}Th activities were always lower than ^{238}U activities (~2.4 dpm L^{-1}) across all stations indicating particle export (Fig. 4). However, the magnitude and extent of the ^{234}Th deficits showed variability. The lowest ^{234}Th activities were found in surface waters of East 1, with average activities of 1.6 ± 0.2 dpm L^{-1}, compared to Station 28, Central and East 2, where average surface activities were 1.9–2.0 dpm L^{-1}. ^{234}Th activities reached equilibrium with ^{238}U at depths between 55 and 100 m, i.e., between the MLD and the base of the PPZ (Fig. 4). The only exception is Station 7 (East 2), the last station to be occupied, where equilibrium was only reached at ~150 m, below the PPZ.

In general, ^{234}Th and ^{238}U activities remained close to each other below the equilibrium depth. However, there were two notable exceptions. At some stations (i.e., East 1 Stations 9 and 12, and Station 28-1), large ^{234}Th activity excesses relative to ^{238}U were apparent within the PPZ, which is indicative of remineralization or disaggregation processes. In addition, we found a ^{234}Th deficit below the PPZ at Station 28-2, which can indicate particle repackaging processes.

One-dimensional (1D) steady state ^{234}Th fluxes (Fig. S5 in the Supplement) reflected the variability observed in ^{234}Th/^{238}U profiles. At the base of the PPZ, ^{234}Th fluxes ranged from negligible in East 1 to 1640 dpm m^{-2} d^{-1} in Central. On average, ^{234}Th fluxes (dpm m^{-2} d^{-1}) at the base of the PPZ were 620 ± 330 in East 1, 360 ± 20 at Station 28, 1290 ± 500 in Central and 820 ± 260 in East 2. In general, considering all stations, ^{234}Th fluxes increased slightly from the base of the PPZ to 100 m below the base (1.4-fold on average), and that increase was most pronounced (2.8-fold) at Station 28-2 due to the ^{234}Th deficit observed below the PPZ at this station (Fig. 4). At 500 m, ^{234}Th fluxes were moderately high, with fluxes ≥1000 dpm m^{-2} d^{-1} at most stations except three stations located outside the central region (Stations 9, 28-1, 15).

3.3. C/Th and bSi/Th in particles

C/Th ratios in >51 µm particles decreased 10-fold with depth from values of up to 41 µmol dpm^{-1} at 40 m to values as low as 4.0 µmol dpm^{-1} at 490 m (Fig. 5). The highest C/Th ratios were found within the PPZ in East 1 where *Phaeocystis* dominated the phytoplankton community and phytoplankton biomass, and NPP rates were highest (Fig. 3). Below the PPZ, C/Th ratios decreased with depth from 13.5 ± 2.8 µmol dpm^{-1} at 115–185 m to 7.1 ± 2.7 µmol dpm^{-1} at 465–490 m considering all stations.

bSi/Th ratios in >51 µm particles also showed a general decrease with depth, but not as marked as C/Th ratios (Fig. 5). The highest bSi/Th ratios throughout all depths were found in East 2, with values decreasing from 2.3–2.7 µmol dpm^{-1} in the upper 220 m to 1.6–1.9 µmol dpm^{-1} at deeper depths. In East 1, Station 28 and Central, bSi/Th ratios decreased from 1.5 ± 0.1 µmol dpm^{-1} at 115–185 m to 1.1 ± 0.1 µmol dpm^{-1} at 465–490 m.

3.4. POC and bSi fluxes

POC flux profiles show large station-to-station variability (Fig. 6a). At the base of the PPZ, POC fluxes ranged by 1 order of magnitude from 2.9 mmol C m^{-2} d^{-1} in East 1 to 22.1 mmol C m^{-2} d^{-1} in Central (Table 1). On average, POC fluxes (mmol C m^{-2} d^{-1}) at the base of the PPZ were 8.4 ± 4.5 in East 1, 4.9 ± 0.2 at Station 28, 17.3 ± 6.7 in

https://doi.org/10.5194/egusphere-2025-3671
Preprint. Discussion started: 25 August 2025

Central and 11.1 ± 3.5 in East 2 (Fig. 6a, 7). POC fluxes at 100 m below the PPZ were not significantly different than those at the base of the PPZ (*t* test, $p > 0.05$), indicating negligible attenuation in POC fluxes below the PPZ and a transfer efficiency close to 1 (i.e., flux at 100 m below PPZ base ~ flux at PPZ base; Fig. 7). At 500 m, POC fluxes were, on average, 8.9 ± 4.2 in East 1, 3.8 ± 4.1 at Station 28, 13.2 ± 5.3 in Central and 6.9 ± 3.7 mmol C m^{-2} d^{-1} in East 2. Only East 2 showed consistent flux attenuation (30–60%) between the base of the PPZ and 500 m at all stations.

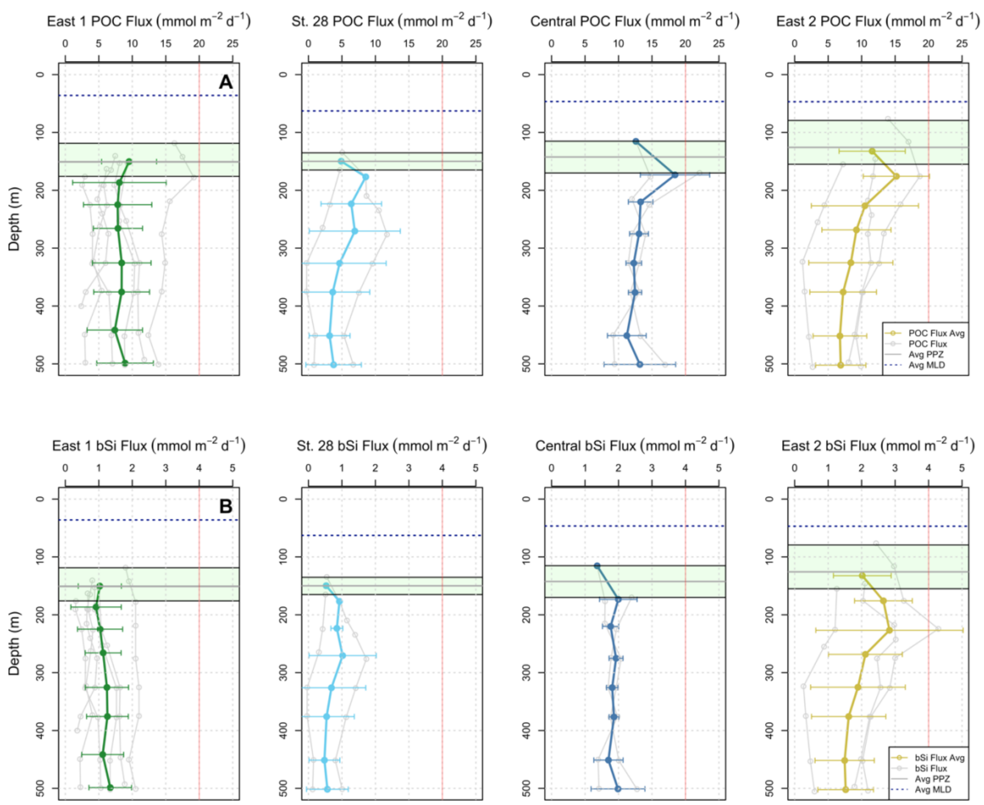

Figure 6. Profiles of particulate organic carbon (POC, panel A) and biogenic silica (bSi, panel B) flux across regions. Fluxes measured at individual stations are shown in grey, whereas averages are shown in color (green for East 1, light blue for St. 28, dark blue for Central, yellow for East 2). The vertical red lines at 20 mmol C m^{-2} d^{-1} for POC and 4 mmol Si m^{-2} d^{-1} for bSi are for visual reference. The base of the primary production zone (PPZ) is shown with green shading (grey solid line indicates the average, black solid lines indicate the minimum and maximum) and the average base of the mixed layer (MLD) is shown with a blue dashed line.

bSi flux profiles also show large variability across stations (Fig. 6b). At the base of the PPZ, bSi fluxes ranged by 1 order of magnitude from 0.3 mmol Si m^{-2} d^{-1} in East 1 to 2.4 mmol Si m^{-2} d^{-1} in Central and East 2 (Table 1). On average, bSi fluxes (mmol Si m^{-2} d^{-1}) at the base of the PPZ were 0.9 ± 0.5 in East 1, 0.5 ± 0.0 at Station 28, 1.9 ± 0.7 in Central and 1.9 ± 0.6 in East 2 (Fig. 6b, 7). In deeper waters at most stations, bSi fluxes were similar

https://doi.org/10.5194/egusphere-2025-3671
Preprint. Discussion started: 25 August 2025

or even higher than at the base of the PPZ indicating either no flux attenuation or addition of bSi at depth. The exception is East 2, where bSi flux attenuated by 10–50% from the base of the PPZ to 500 m.

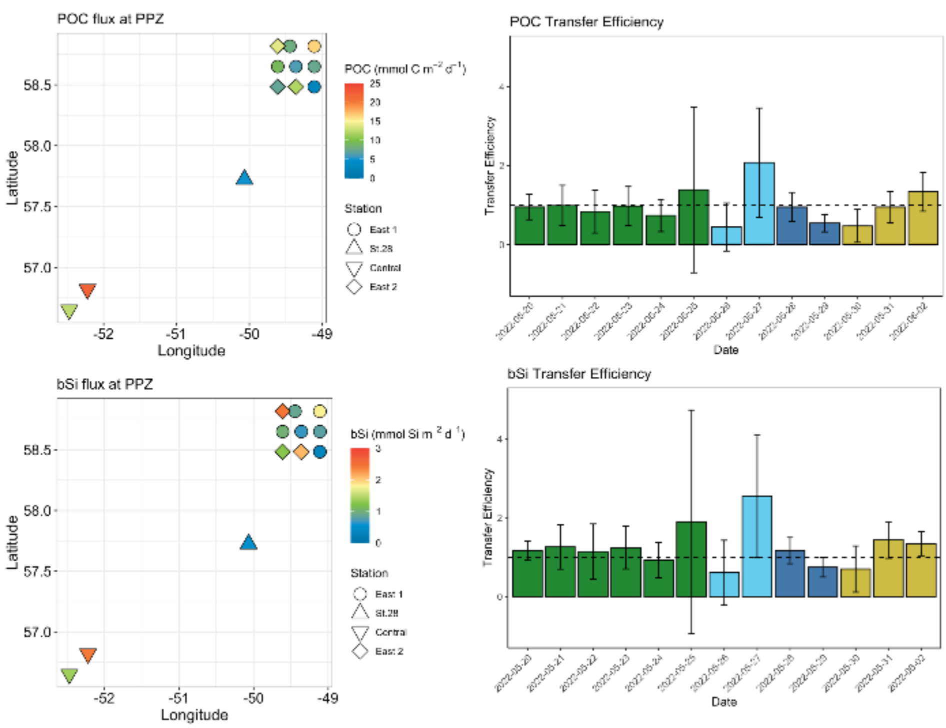

Figure 7. Spatial maps of particulate organic carbon (POC) and biogenic silica (bSi) flux at the base of the primary production zone (PPZ, left panels) and transfer efficiency (flux at 100 m below PPZ base/flux at PPZ base) of POC and bSi over time in the study area (right panels). The horizontal dashed lines in the right panels indicate a transfer efficiency = 1.

3.5. Comparison with other studies

Only three prior studies have used ^{234}Th to estimate POC fluxes in the Labrador Sea: Moran et al. (2003) in July 1999 (three stations), Puigcorbé et al. (2017) in early May 2010 (one station), and Lemaitre et al. (2018) in late June 2014 (three stations), the last one during the decline of a diatom bloom. The ^{234}Th flux results from our study are similar to those obtained at the PPZ base (or at 100 m, Moran et al., 2003) in June (700–860 dpm m^{-2} d^{-1}, Lemaitre et al. 2018) and lie between the fluxes measured in May (270 dpm m^{-2} d^{-1}, Puigcorbé et al. 2017) and later in the season in July (980–1400 dpm m^{-2} d^{-1}, Moran et al. 2003). Regarding POC fluxes, our fluxes are 1 order of magnitude higher than those measured in early May (0.6 mmol C m^{-2} d^{-1}, Puigcorbé et al., 2017), but encompass the range of POC fluxes measured in June (6.1–10 mmol C m^{-2} d^{-1}, Lemaitre et al., 2018) and July (5.7–21 mmol C m^{-2} d^{-1}, Moran et al., 2003). The vertical flux attenuation of POC found in this study is lower than that measured in June (Lemaitre et al., 2018) when a ~40–70% flux attenuation between the base of the PPZ and 100 m below the PPZ base was found (vs. no flux attenuation in this study). On the other hand, our bSi fluxes

https://doi.org/10.5194/egusphere-2025-3671
Preprint. Discussion started: 25 August 2025

are lower (3 to 5-fold) than those measured by Lemaitre (2017) close to the base of the PPZ but similar or even higher than their fluxes at 400 m (negligible–0.9 mmol Si m^{-2} d^{-1}).

Compared to other *Phaeocystis* blooms, our ^{234}Th flux results from the Eastern Grid, where the decline of an extensive *Phaeocystis* bloom was occurring, lie in the lower range of other *Phaeocystis* blooms that reported fluxes of up to 3000–4000 dpm m^{-2} d^{-1} at the ice edge in the Fram Strait (Le Moigne et al., 2015) and in the marginal ice zone of the Barents Sea (Lalande et al., 2008). Regarding POC fluxes in other *Phaeocystis* blooms (Table 2), our POC fluxes in the Eastern Grid compare well with those found in the Barents Sea using sediment traps (Lalande et al., 2008), but are lower than those measured in that same study using ^{234}Th and large volume sampling. Our POC fluxes in the Eastern Grid are also lower (2 to 8-fold) than those reported in a number of other Arctic and sub-Arctic studies during *Phaeocystis* blooms (Coppola et al., 2002; Dybwad et al., 2021; Le Moigne et al., 2015; Reigstad and Wassmann, 2007). Compared to studies that reported blooms dominated by both *Phaeocystis* and diatoms (Table 2), our POC fluxes fall within the range of those measured in the Crozet Plateau (Morris et al., 2007; Salter et al., 2007), but are lower (4-fold) than those reported in the Barents Sea (Andreassen and Wassmann, 1998) and the Ross Sea (Asper and Smith, 1999). Our bSi fluxes are also lower (4 to 9-fold) than those measured in the Crozet Plateau (Salter et al., 2007).

https://doi.org/10.5194/egusphere-2025-3671
Preprint. Discussion started: 25 August 2025

Table 2. Compilation of sinking fluxes and biological carbon pump efficiency metrics in *Phaeocystis* and diatom blooms. Values given in parentheses next to ranges indicate averages. PPZ = primary production zone, PAR = photosynthetic active radiation, Eq depth = ^{234}Th and ^{238}U equilibrium depth, NPP = net primary production, POC = particulate organic carbon, bSi = biogenic silica, ISP = in situ pump, ST = sediment trap.

Study area	Reference depth z (m)	Integrated NPP (mmol C m^{-2} d^{-1})	POC flux at z (mmol C m^{-2} d^{-1})	Export efficiency (%)	Transfer efficiency z+100 m (%)	bSi flux at z (mmol Si m^{-2} d^{-1})	Molar bSi/POC at z	Bloom stage	Dominant species	Flux method	Number of stations considered	References
Labrador Sea	119–176 (PPZ)	125–252 (188)	2.9–16 (8.4)	2–9 (6)	74–139 (98)	0.3–1.8 (0.9)	0.1	Bloom decline	*Phaeocystis*	^{234}Th + ISPs	n = 6, East 1	This study
	79–155 (PPZ)	39–43 (41)	7.2–14 (11)	31–33 (32)	48–134 (92)	1.3–2.4 (1.9)	0.2	Post-bloom			n = 3, East 2	
Fram Strait	100	59 ± 2	78 ± 9	130 ± 30	–	–	–	After bloom peak	*Phaeocystis*	^{234}Th + ISP	n = 1	Le Moigne et al. 2015
	100	48–64 (56)	6.8–13 (9.8)	11–30 (21)	–	–	–	During/after bloom peak	Diatoms		n = 2	
Barents Sea	60	–	14–62 (33)	–	–	–	–	Early bloom/bloom /late bloom	*Phaeocystis*	^{234}Th + large volume sampling	n = 5	Lalande et al. 2008
	60	–	5.6–19 (12)	–	–	–	–			Drifting STs		
Barents Sea	90	–	17	–	–	–	–	Bloom	*Phaeocystis*	Drifting STs	n = 1	Coppola et al. 2002
Barents Sea	40 (0.1%PAR)	67–76 (71)	35–48 (42)	47–72 (59)	56–78 (67)	–	–	Early bloom	*Phaeocystis* and diatoms	Drifting STs	n = 2	Andreassen and Wassmann 1998; Buesseler et al. 2020
	35 (0.1%PAR)	68	54	79	41	–	–	Well-developed bloom	Diatoms		n = 1	
North Norwegian fjords & Barents Sea	90–100	–	15–64 (40)	–	–	–	–	Bloom and after bloom	*Phaeocystis*	Drifting STs	Average of several stations and cruises	Reigstad and Wassmann 2007
North of Svalbard	50	–	13–33 (23)	–	–	–	–	Bloom	*Phaeocystis*	Ice-tethered STs	n = 6	Dybwad et al. 2021
	60	–	15–47 (34)	–	–	–	–		Diatoms		n = 4	
Ross Sea	50	49–206 (105)	21–66 (34)	21–44 (34)	15–50 (35)	–	–	After bloom peak	*Phaeocystis* and diatoms	Drifting STs	n = 5	Asper and Smith 1999
Crozet Plateau, Southern Ocean	87–248	–	1.0–17 (4.8)	–	–	0.3–29 (7.9)	0.2–2.8 (1.4)	Bloom decline	*Phaeocystis* and diatoms	Neutrally buoyant STs	n = 3 + reoccupations	Salter et al. 2007
	101–204	10–250 (70)	4.9–30 (17)	7–305 (54)	–	–	–			^{234}Th + ISPs	n = 8 + reoccupations	Morris et al. 2007
Labrador Sea	40–80 (Eq depth & PPZ; ± 5)	27–80 (54)	6.1–10 (8.0)	8–38 (20)	30–63 (48)	2.7–6.6 (4.8)	0.4–0.8 (0.6)	After bloom peak	Diatoms	^{234}Th + ISPs	n = 3	Lemaitre et al. 2018; Lemaitre 2017
Porcupine Abyssal Plain	67–133 (PPZ)	54–90 (75)	9.1–14 (11)	8–26 (16)	107–155 (139)	3.4–6.1 (4.4)	0.3–0.4 (0.4)	Bloom decline	Diatoms	^{234}Th + ISPs	n = 23	Clevenger et al. 2024
Atlantic sector Southern Ocean	100–120	66–234 (153)	11–44 (19)	7–34 (12)	–	–	–	Bloom decline	Diatoms	Drifting STs	n = 11	Roca-Martí et al. 2017
Kerguelen Plateau, Southern Ocean	100	82	23 ± 4	28	107	–	–	Bloom decline	Diatoms	^{234}Th + hose pump & drifting STs	n = 1 + reoccupations	Savoye et al. 2008

4. Discussion

4.1. POC fluxes in the central Labrador Sea during the decline of a *Phaeocystis* bloom

This study presents an unprecedented number of measurements of sinking fluxes in the central Labrador Sea (~300 ^{234}Th measurements) and represents one of the largest assessments of the impact of *Phaeocystis* blooms on POC export. Data collected by Fisheries and Oceans Canada along the Atlantic Repeat Hydrography Line 7 West (AR7W) as part of the Atlantic Zone Off-shelf Monitoring Program (AZOMP) between 2014 and 2022, revealed that the *Phaeocystis* bloom encountered in this study (spring 2022) was unusual given its large spatial extent and high biomass concentration (Devred et al., 2024, 2025). Using satellite remote sensing data combined with an ecological approach, these authors determined that the 2022 *Phaeocystis* bloom extended over more than half of the Labrador Sea, lasted for 6 weeks, and resulted in a remarkably high total primary production that accounted for 60% of the May production in the Labrador Sea (33.2 Tg C; Devred et al., 2025). Genomic analyses conducted

https://doi.org/10.5194/egusphere-2025-3671
Preprint. Discussion started: 25 August 2025

during our expedition, 1 week later than the 2022 AZOMP mission, confirmed that the species of this bloom was *Phaeocystis pouchetii* (Bertrand et al., in prep).

The sampling of the *Phaeocystis* bloom in this study mostly focused on a ~1075 km^2 grid (Eastern Grid) at the southern edge of the bloom about 2 to 3 weeks after its peak. The stations sampled from 20 May to 25 May (East 1) showed integrated NPP rates that were, on average, five times higher than those sampled from 30 May to 2 June (East 2) (Table 1) which were considered to represent post-bloom conditions (Bertrand et al., in prep). Two stations located to the southwest of the Eastern Grid outside of the bloom (Central) were also sampled and represented more typical conditions of the central Labrador Sea with a mixed phytoplankton community composition that was more diatom dominated (Devred et al., 2024, 2025). Beyond the Eastern grid, another station (Station 28) was also sampled in the *Phaeocystis* bloom area, but no in situ NPP data were collected at that station. For this reason, below we focus our discussion on the Eastern Grid and Central (inside vs. outside of the major *Phaeocystis* bloom).

POC fluxes at the base of the PPZ were, overall, moderate to high, but POC fluxes in the *Phaeocystis* bloom were lower than those measured outside of the bloom, with average fluxes of 8 and 11 mmol C m^{-2} d^{-1} in East 1 and East 2, respectively, and 17 mmol C m^{-2} d^{-1} in Central. This indicates that the decline of the extensive bloom sampled during this study did not enhance POC export. In general, POC fluxes did not decrease from the base of the PPZ to 500 m, except for East 2 where all stations showed a consistent decrease (30–60%). This resulted in POC fluxes at 500 m that were on average 9 and 7 mmol C m^{-2} d^{-1} in East 1 and East 2, respectively, and 13 mmol C m^{-2} d^{-1} in Central, showing lower fluxes in the *Phaeocystis* bloom region also at depth. Despite the limited flux attenuation found in the upper mesopelagic, taken together, these findings suggest a limited role of *Phaeocystis* in export.

Phaeocystis spp. play an exceptional role in marine ecosystems due to its high carbon content when blooming and because of its unique polymorphic life cycle, including free-living cells of <10 µm and gelatinous colonies that usually reach sizes of several mm (Schoemann et al., 2005). However, despite the large sizes of *Phaeocystis* colonies, most of the literature available on the topic shows that *Phaeocystis*-derived material is largely recycled in the upper ocean (Smith and Trimborn, 2024 and references therein). For instance, a compilation of sediment trap studies, including data ranging from polar to sub-Arctic and boreal regions, revealed that *Phaeocystis* POC fluxes strongly decline throughout the upper 100 m of the water column (Reigstad and Wassmann, 2007). Our observations of large excesses of ^{234}Th relative to ^{238}U at around 70–100 m in the Eastern Grid (Stations 9 and 12) and Station 28-1 (Fig. 4) also support shallow remineralization of sinking particles during *Phaeocystis* blooms. Yet, *Phaeocystis*-derived material can be efficiently exported to depth under certain circumstances, including: the formation of aggregates by *Phaeocystis* colonies facilitated by the release of transparent exopolymer particles (TEP) which can scavenge other particles like ballasting minerals (Andreassen and Wassmann, 1998; Passow and Wassmann, 1994; Wollenburg et al., 2018); and through physical mixing processes, such as downwelling associated with eddy activity (Lalande et al., 2011). The incorporation of *Phaeocystis* into fast-sinking zooplankton pellets has also been identified as an important export pathway (Dybwad et al., 2021; Wiedmann et al., 2020).

https://doi.org/10.5194/egusphere-2025-3671
Preprint. Discussion started: 25 August 2025

4.2. Why did this *Phaeocystis* bloom not lead to enhanced fluxes?

Our observations during the decline of a massive *Phaeocystis* bloom in the Labrador Sea do not show indications of enhanced sinking fluxes when compared to an area located outside of the major bloom. These observations cover a period of 2 weeks during which NPP in the bloom area strongly declined, but POC fluxes remained relatively constant. As described in Sect. 2.5, the assumptions behind the ^{234}Th export model used in this study have been assessed and validated to the best of our possibilities based on information of the dynamics specific to that bloom and a hindcast simulation of physical transport at the time of the cruise. Furthermore, the conversion from ^{234}Th to POC fluxes using >51 µm particles from large volume filtration in this study is supported with independent data from marine snow catchers (see Sect. 2.4). We also note that the C/Th ratios used to estimate POC fluxes in this study (≤ 16 µmol dpm^{-1}) are far below the ratios measured by Lalande et al. (2008) of up to >100 µmol dpm^{-1} which were considered to be biased towards high values and in turn led to overestimated POC-derived fluxes. Hence, the comparison of our data with context information and independent methods gives confidence in the export estimates presented here.

One hypothesis for the lack of enhanced sinking fluxes is that *Phaeocystis* material resulting from the decline of the bloom was not sufficiently ballasted. *Phaeocystis* colonies can release large amounts of TEP during their growth and their senescence, which, thanks to the high stickiness of TEP, can aggregate suspended particles and facilitate the formation of marine snow (Passow, 2002). However, the density of TEP is lower than that of seawater, which may cause the aggregates to remain in surface waters if not ballasted by other particles (Mari et al., 2017). In line with this, other studies have shown that below the mixed layer, marine biogels such as TEP can adhere to and accumulate on particles, reducing their sinking velocity by increasing both their buoyancy and hydrodynamic resistance, which may enhance carbon flux attenuation (Alcolombri et al., 2025; Romanelli et al., 2023). Sinking rates of *Phaeocystis* colonies and aggregates range from negligible to up to 200 m d^{-1} (Schoemann et al., 2005), indicating that their capacity to sink and get transferred from the upper ocean to depth depends on their characteristics including the amount and type of particles that might have been scavenged. For instance, in the ice-covered Arctic Ocean, sinking of *Phaeocystis* aggregates throughout the water column down to the seafloor has been associated with ballasting by cryogenic gypsum which would have increased the density of such aggregates, facilitating their export to abyssal depths (Wollenburg et al., 2018). More common ballasting minerals that are known to increase the density of phytoplankton aggregates and enhance their export include continental dust, calcium carbonate, and biogenic silica (Armstrong et al., 2002). Yet, to our knowledge, the role of those minerals in controlling the sinking of *Phaeocystis* aggregates have not been explored.

In this study, we measured both POC and bSi fluxes. Molar bSi to POC ratios in particles >51 µm within the PPZ were lower in East 1 (0.02–0.08) relative to those in Central (0.13) and East 2 (0.15–0.20), which agrees with phytoplankton community composition data from the cruise showing a lower relative contribution of diatoms to biomass in East 1 (Bertrand et al., in prep). Likewise, bSi fluxes at the base of the PPZ were 2-fold lower in East 1 than in Central and East 2 (Table 1), indicating a smaller contribution of siliceous plankton to export flux in East 1. However, below the PPZ, bSi fluxes in East 1 and East 2 became more similar, with fluxes within the same range at 500 m. Overall, bSi/POC ratios were relatively low in all areas, with averages from the base of the PPZ down to 500 m of 0.14 ± 0.03 (East 1), 0.18 ± 0.06 (Central), and 0.22 ± 0.04 (East 2).

https://doi.org/10.5194/egusphere-2025-3671
Preprint. Discussion started: 25 August 2025

To our knowledge, bSi/POC ratios during the decline of other *Phaeocystis* blooms have not been reported. Our bSi/POC ratios fall in the lower range of those measured in the Labrador Sea (Lemaitre et al., 2018), the Porcupine Abyssal Plain (Clevenger et al., 2024), and the Crozet Plateau (Salter et al., 2007) during the decline of either diatom or mixed diatom and *Phaeocystis* blooms (Table 2). The bSi/POC ratios measured in this study are also lower than those found in the upper mesopelagic of Ocean Station Papa during low flux conditions (0.63 ± 0.28; Roca-Martí et al., 2021). Taken together, these results suggest that sinking particles during the BELAS-1 expedition were not heavily ballasted with bSi or, in other words, that diatoms did not appear to play an important ballasting role, which could at least partly explain the limited export of *Phaeocystis* in this study.

Other factors that may help explain why this *Phaeocystis* bloom did not lead to enhanced fluxes will be assessed elsewhere, including the analysis of the biochemical composition and morphology of suspended and sinking particles (Cisternas-Novoa et al., in prep.) or their susceptibility to be degraded by heterotrophic bacteria (Romanelli et al., in prep.).

4.3. BCP efficiency

The export efficiency (i.e., flux at PPZ base/integrated NPP within PPZ) and transfer efficiency (i.e., flux at 100 m below PPZ base/flux at PPZ base) are two common metrics for assessing the efficiency of the biological carbon pump and allowing comparisons between studies across different regions and seasons (Buesseler et al., 2020; Buesseler and Boyd, 2009). Here, we obtain export efficiencies ranging from 2 to 9% in East 1 and 31 to 33% in East 2 using in situ estimates of integrated NPP throughout the PPZ in combination with POC flux estimates measured at the base of that layer (Table 1, 2). Transfer efficiencies ranged from 48 to 139% and were on average 98% in East 1 and 92% in East 2 suggesting that flux attenuation throughout the upper 100 m of the mesopelagic zone was low. Combining both metrics, we obtain an overall BCP efficiency, defined as the amount of NPP reaching 100 m below the PPZ base, of 6% in East 1 and 29% in East 2. That would place this *Phaeocystis* bloom in the Labrador Sea as either a low BCP efficiency system (when looking at East 1 results) like the oligotrophic site ALOHA near Hawaii (Buesseler and Boyd, 2009), or a high BCP efficiency system (when looking at East 2 results) similar to that found in the Kerguelen Plateau (Savoye et al., 2008) and in the Barents Sea (Andreassen and Wassmann, 1998; Buesseler et al., 2020) during diatom and mixed diatom and *Phaeocystis* blooms (Fig. 8, Table 2).

https://doi.org/10.5194/egusphere-2025-3671
Preprint. Discussion started: 25 August 2025

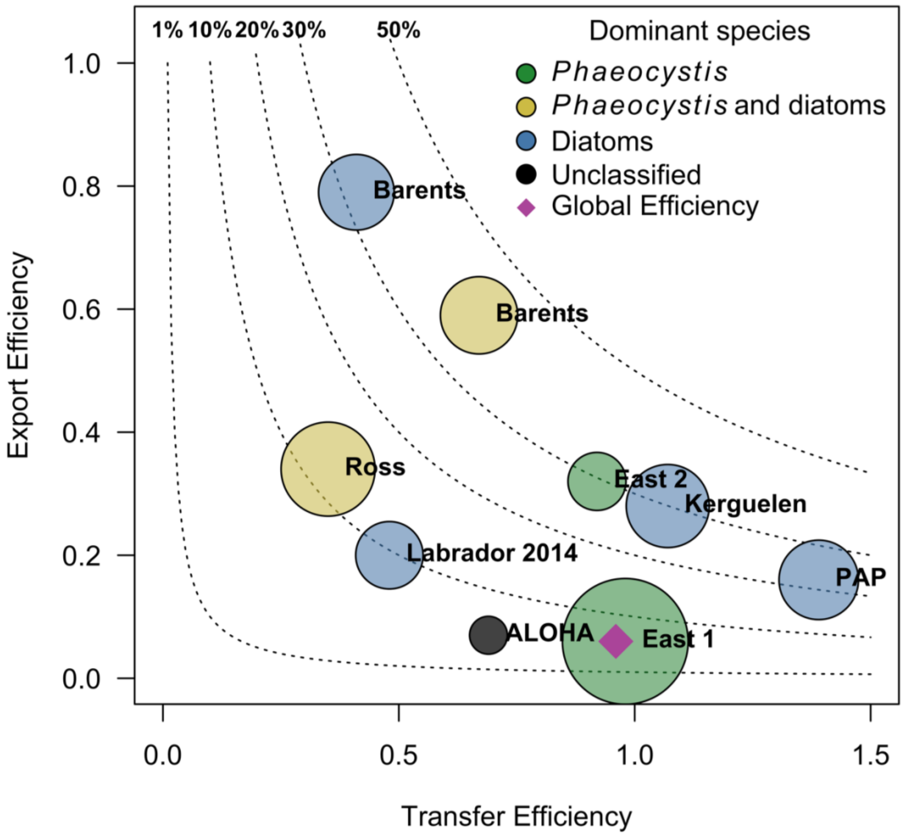

Figure 8. Biological carbon pump efficiency (BCP) comparing bloom studies across different regions (see Table 2). The x-axis depicts transfer efficiency (flux at 100 m below PPZ base/flux at PPZ base) and the y-axis export efficiency (flux at PPZ base/integrated NPP within PPZ). Contour lines are overall BCP efficiency (percentages), and symbol area is proportional to NPP. The "East 1" and "East 2" symbols and the diamond correspond to this study. Studies are colour coded corresponding to the dominant phytoplankton species. The ALOHA site (Buesseler and Boyd, 2009) is also shown as a low-end member. PPZ = primary production zone, NPP = net primary production.

Yet, these BCP metrics are based on NPP and export estimates measured during the same time window. Given the similar POC fluxes measured in East 1 and East 2, the increase in export efficiencies observed with time in the Eastern Grid, from East 1 to East 2, is due to a decrease in NPP with time. This increase in export efficiencies may reflect either 1) a more efficient BCP during post-bloom conditions, or more likely 2) a temporal decoupling between primary production and export (Henson et al., 2015) which have been shown to explain the inverse relationship between NPP and export efficiency found in different oceanic regions (Laws and Maiti, 2019; Roca-Martí et al., 2017). In other words, in this study, the export measured during post-bloom conditions in East 2, when NPP was low, could have been fueled with higher NPP rates that occurred at an earlier phase of the bloom. It is important to keep in mind that the NPP rates presented in this study were measured in the late stages of the

https://doi.org/10.5194/egusphere-2025-3671
Preprint. Discussion started: 25 August 2025

bloom during its decline (East 1) and post-bloom phase (East 2) and therefore do not reflect the higher rates that occurred before the field campaign.

In order to estimate a global BCP efficiency for the 2022 *Phaeocystis* bloom in the Labrador Sea (see diamond in Fig. 8), where NPP and export estimates are compared over longer timescales (Laws and Maiti, 2019), we have used satellite-derived NPP (Devred et al., 2025) in the Eastern Grid area from the peak of the *Phaeocystis* bloom until the last sampling day of the BELAS-1 expedition (9 May–2 June, Fig. S6 in the Supplement). We have obtained an integrated NPP during that period of 3920 mmol C m^{-2} which, combined with the POC fluxes measured in the Eastern Grid (average of 9.3 mmol C m^{-2} d^{-1} in East 1 and 2) multiplied by 25 d (i.e., 232 mmol C m^{-2}), results in a global export efficiency for the *Phaeocystis* bloom decline of 6%. This estimate assumes that the POC export measured in East 1 and 2 using ^{234}Th (half-life = 24.1 d) is representative of the export that occurred over the 25 d from the peak of the bloom until the end of the bloom. Using that export efficiency combined with an average transfer efficiency in the Eastern Grid of 96% (East 1 and 2), we would obtain an overall BCP efficiency of 6%, which is the same as that obtained in East 1 (Fig. 8). This analysis suggests that East 1 results represent better the overall BCP efficiency of the extensive *Phaeocystis* bloom occurred in the Labrador Sea in spring 2022 and stresses the importance of long-term observations of the BCP. The overall BCP efficiency obtained in this study is lower than that reported during other blooms in the North Atlantic and Southern Ocean, dominated by either diatoms or *Phaeocystis* and diatoms (Fig. 8, Table 2).

Altogether, our findings highlight the complexity of quantifying the contribution of phytoplankton blooms to carbon export and underscore the importance of sustained observations to better capture their variability and broader implications in a changing ocean. This study provides a foundation for future comparisons with other datasets from the BELAS-1 expedition. Integrating these datasets will help elucidate the mechanisms underlying low BCP efficiency events, such as the one observed during this study, thereby improving our ability to predict the consequences of shifting bloom dynamics for global carbon export. Moreover, future efforts will offer the opportunity to extend the observational period by incorporating data from autonomous platforms, thereby shedding light on the evolution of sinking fluxes beyond the limited timeframe of ship-based campaigns.

5. Conclusions

This study represents one of the largest assessments ever of the impact of *Phaeocystis* blooms on sinking fluxes using ^{234}Th as a tracer during a 2-week-long process study in spring 2022. The *Phaeocystis* bloom encountered was unusually large and highly productive extending over more than half of the Labrador Sea for 6 weeks. The main conclusions of this work are summarized below:

- During the late stages of the bloom, POC fluxes in the upper mesopelagic down to 500 m were variable but overall moderate to high (average of 8 ± 5 mmol C m^{-2} d^{-1}). Yet, evidence of shallow POC flux remineralization combined with the fact that POC fluxes in the bloom were not higher than in a region sampled outside of the bloom (average of 13 ± 3 mmol C m^{-2} d^{-1}) suggests a limited role of *Phaeocystis* in carbon export.

- Large (>51 µm) particles collected using large volume pumps presented relatively low bSi/POC ratios and, therefore, diatoms did not appear to have an important ballasting role of *Phaeocystis*-derived material during the observation period.
- 2 weeks after the peak of the bloom, the total amount of in situ NPP that reached 100 m below the euphotic zone was only 6%. However, 3 weeks after the peak of the bloom, the value had increased to 29%. This apparent change was driven primarily by a decline in NPP over the sampling period, highlighting how sensitive the BCP efficiency determination is to temporal changes in NPP.
- Using satellite-derived NPP from the peak of the bloom until its end, we obtain an overall BCP efficiency of 6% supporting a low BCP efficiency system. We stress the importance of long-term observations of both NPP and POC export for estimating meaningful BCP efficiencies. Future research including data from autonomous platforms will elucidate how sinking fluxes might have changed after this ship-based observation study.
- The BCP efficiency of this *Phaeocystis* bloom is clearly lower than that found during the decline of either diatom blooms or mixed diatom and *Phaeocystis* blooms (albeit with no bSi/POC information) in the North Atlantic and Southern Ocean.
- To elucidate under which conditions *Phaeocystis* can be a good exporter, future research should include the analysis of bSi and other ballasting minerals, if possible, in all particle size fractions. These measurements will be key to shedding light on the role of the BCP in sequestering carbon in a future ocean where small cells, such as *Phaeocystis*, will increasingly dominate phytoplankton communities (Finkel et al., 2010; Passow and Carlson, 2012).

Data availability. Thorium-234 (^{234}Th) and size-fractionated particulate data were published open access (Roca-Martí et al., 2025a, b).

Author contributions. SK contributed to funding acquisition. MRM, MH, SK contributed to the experimental conceptual design. All authors contributed to data generation and analysis. MRM, MH, CM, SK contributed to the initial manuscript draft (MH data visualization), and all co-authors contributed to the revision of the paper.

Competing interests. The authors declare that they have no conflict of interest.

Acknowledgements. This work is dedicated to Markus Kienast, a dear colleague whose approach to both science and life deeply inspires us all. We will always remember his passion, enthusiasm, positivity, and sense of humor. This study is part of the Ocean Frontier Institute's research project "The Northwest Atlantic Biological Carbon Pump" (NWA-BCP). We are sincerely grateful to the crew and scientific party aboard the RV *Celtic Explorer* during the BELAS-1 expedition and the whole NWA-BCP team. We would like to acknowledge Maria Armstrong (^{234}Th team), and Britton Dempsey and Brianna Stanley (NPP team) for their invaluable help with the expedition's preparation, sample collection and/or processing. We also thank Stephanie Clay for providing satellite data, Gretchen Swarr and Claire Normandeau for measuring ^{230}Th/^{229}Th and POC, and Ken Buesseler and Uta Passow for providing insightful discussions about the data. We thank OBPG-NASA for making satellite ocean colour data available and the support from the DFO Atlantic Zone Off-shelf Monitoring Program to collect in situ data used to develop satellite-based data products.

Financial support. MRM acknowledges support from the Ocean Frontier Institute (OFI) International Postdoctoral Fellowship Program, the Beatriu de Pinós Fellowship (2021-BP-00109), the "la Caixa" Foundation (ID 100010434, fellowship code LCF/BQ/PI24/12040022), the ICTA-UAB "María de Maeztu" Program for Units of Excellence of the Spanish Ministry of Science and Innovation (CEX2024-001506-M funded by MICIU/AEI

/10.13039/501100011033), and ICTA-UAB MERS (2021 SGR-640) of the Generalitat de Catalunya. MH was supported by the Nova Scotia Graduate Scholarship (NSGS), and SK by the Natural Sciences and Engineering Research Council of Canada (NSERC) and OFI.

References

Alcolombri, U., Nissan, A., Słomka, J., Charlton, S., Secchi, E., Short, I., Lee, K. S., Peaudecerf, F. J., Baumgartner, D. A., Sichert, A., Sauer, U., Sengupta, A., and Stocker, R.: Biogel scavenging slows the sinking of organic particles to the ocean depths, Nat. Commun. 2025 161, 16, 1–10, https://doi.org/10.1038/s41467-025-57982-5, 2025.

Andreassen, I. J. and Wassmann, P.: Vertical flux of phytoplankton and particulate biogenic matter in the marginal ice zone of the Barents Sea in May 1993, Mar. Ecol. Prog. Ser., 170, 1–14, https://doi.org/10.3354/MEPS170001, 1998.

Armstrong, R. A., Lee, C., Hedges, J. I., Honjo, S., and Wakeham, S. G.: A new, mechanistic model for organic carbon fluxes in the ocean based on the quantitative association of POC with ballast minerals, Deep Sea Res. Part II Top. Stud. Oceanogr., 49, 219–236, https://doi.org/10.1016/S0967-0645(01)00101-1, 2002.

Arruda, R., Atamanchuk, D., Boteler, C., and Wallace, D. W. R.: Seasonality of pCO_2 and air-sea CO_2 fluxes in the Central Labrador Sea, Front. Mar. Sci., 11, 1472697, https://doi.org/10.3389/fmars.2024.1472697, 2024.

Asper, V. L. and Smith, W. O.: Particle fluxes during austral spring and summer in the southern Ross Sea, Antarctica, J. Geophys. Res. Ocean., 104, 5345–5359, https://doi.org/10.1029/1998JC900067, 1999.

Baker, C. A., Martin, A. P., Yool, A., and Popova, E.: Biological Carbon Pump Sequestration Efficiency in the North Atlantic: A Leaky or a Long-Term Sink?, Global Biogeochem. Cycles, 36, e2021GB007286, https://doi.org/10.1029/2021GB007286, 2022.

Baltar, F., Arístegui, J., Gasol, J. M., Sintes, E., and Herndl, G. J.: Evidence of prokaryotic metabolism on suspended particulate organic matter in the dark waters of the subtropical North Atlantic, Limnol. Oceanogr., 54, 182–193, https://doi.org/10.4319/LO.2009.54.1.0182, 2009.

Baumas, C., Fuchs, R., Garel, M., Poggiale, J.-C., Memery, L., Le Moigne, F. A. C., and Tamburini, C.: Reconstructing the ocean's mesopelagic zone carbon budget: sensitivity and estimation of parameters associated with prokaryotic remineralization, Biogeosciences, 20, 4165–4182, https://doi.org/10.5194/BG-20-4165-2023, 2023.

Bishop, J. K. B., Lam, P. J., and Wood, T. J.: Getting good particles: Accurate sampling of particles by large volume in-situ filtration, Limnol. Oceanogr. Methods, 10, 681–710, https://doi.org/10.4319/lom.2012.10.681, 2012.

Boyd, P. W., Sherry, N. D., Berges, J. A., Bishop, J. K. B., Calvert, S. E., Charette, M. A., Giovannoni, S. J., Goldblatt, R., Harrison, P. J., Moran, S. B., Roy, S., Soon, M., Strom, S., Thibault, D., Vergin, K. L., Whitney, F. A., and Wong, C. S.: Transformations of biogenic particulates from the pelagic to the deep ocean realm, Deep Sea Res. Part II Top. Stud. Oceanogr., 46, 2761–2792, https://doi.org/10.1016/S0967-0645(99)00083-1, 1999.

Boyd, P. W., Claustre, H., Levy, M., Siegel, D. A., and Weber, T.: Multi-faceted particle pumps drive carbon sequestration in the ocean, Nature, 568, 327–335, https://doi.org/10.1038/s41586-019-1098-2, 2019.

de Boyer Montégut, C., Madec, G., Fischer, A. S., Lazar, A., and Iudicone, D.: Mixed layer depth over the global ocean: An examination of profile data and a profile-based climatology, J. Geophys. Res., 109, C12003, https://doi.org/10.1029/2004JC002378, 2004.

Buesseler, K. O. and Boyd, P. W.: Shedding light on processes that control particle export and flux attenuation in the twilight zone of the open ocean, Limnol. Oceanogr., 54, 1210–1232, https://doi.org/10.4319/lo.2009.54.4.1210, 2009.

Buesseler, K. O., Boyd, P. W., Black, E. E., and Siegel, D. A.: Metrics that matter for assessing the ocean biological carbon pump, Proc. Natl. Acad. Sci., 117, 9679–9687, https://doi.org/10.1073/PNAS.1918114117, 2020.

Burd, A. B., Hansell, D. A., Steinberg, D. K., Anderson, T. R., Arístegui, J., Baltar, F., Beaupré, S. R., Buesseler, K. O., DeHairs, F., Jackson, G. A., Kadko, D. C., Koppelmann, R., Lampitt, R. S., Nagata, T., Reinthaler, T., Robinson, C., Robison, B. H., Tamburini, C., and Tanaka, T.: Assessing the apparent imbalance between geochemical and biochemical indicators of meso- and bathypelagic biological activity: What the @$♯! is wrong with present calculations of carbon budgets?, Deep Sea Res. Part II Top. Stud. Oceanogr., 57, 1557–1571, https://doi.org/10.1016/j.dsr2.2010.02.022, 2010.

Ceballos-Romero, E., De Soto, F., Le Moigne, F. A. C., García-Tenorio, R., and Villa-Alfageme, M.: ^{234}Th-derived particle fluxes and seasonal variability: when is the SS assumption reliable? Insights from a novel approach for carbon flux simulation, Geophys. Res. Lett., https://doi.org/10.1029/2018GL079968, 2018.

Claustre, H., Legendre, L., Boyd, P. W., and Levy, M.: The Oceans' Biological Carbon Pumps: Framework for a Research Observational Community Approach, Front. Mar. Sci., 8, https://doi.org/10.3389/fmars.2021.780052, 2021.

Clevenger, S. J., Benitez-Nelson, C. R., Drysdale, J., Pike, S., Puigcorbé, V., and Buesseler, K. O.: Review of the analysis of ^{234}Th in small volume (2–4 L) seawater samples: improvements and recommendations, J. Radioanal. Nucl. Chem., 329, 1–13, https://doi.org/10.1007/s10967-021-07772-2, 2021.

Clevenger, S. J., Benitez-Nelson, C. R., Roca-Martí, M., Bam, W., Estapa, M., Kenyon, J. A., Pike, S., Resplandy, L., Wyatt, A., and Buesseler, K. O.: Carbon and silica fluxes during a declining North Atlantic spring bloom as part of the EXPORTS program, Mar. Chem., 258, 104346, https://doi.org/10.1016/J.MARCHEM.2023.104346, 2024.

Coppola, L., Roy-Barman, M., Wassmann, P., Mulsow, S., and Jeandel, C.: Calibration of sediment traps and particulate organic carbon export using ^{234}Th in the Barents Sea, Mar. Chem., 80, 11–26, https://doi.org/10.1016/S0304-4203(02)00071-3, 2002.

Devred, E., Wilson, K. L., Perry, T., Hardy, M., Brosnahan, M., and Ringuette, M.: Identification and validation of phytoplankton taxonomic assemblages derived from pigment signatures using samples collected in the Labrador Sea from 2014 to 2022, Dartmouth, Nova Scotia, Canada, 37 pp., 2024.

Devred, E., Clay, S., Ringuette, M., Perry, T., Amirian, M., Irwin, A., and Finkel, Z.: Net primary production in the Labrador Sea between 2014 and 2022 derived from ocean colour remote sensing based on ecological regimes, Remote Sens. Environ., 323, 114713, https://doi.org/10.1016/J.RSE.2025.114713, 2025.

Dybwad, C., Assmy, P., Olsen, L. M., Peeken, I., Nikolopoulos, A., Krumpen, T., Randelhoff, A., Tatarek, A., Wiktor, J. M., and Reigstad, M.: Carbon Export in the Seasonal Sea Ice Zone North of Svalbard From Winter to Late Summer, Front. Mar. Sci., 7, 525800, https://doi.org/10.3389/fmars.2020.525800, 2021.

Finkel, Z. V., Beardall, J., Flynn, K. J., Quigg, A., Rees, T. A. V., and Raven, J. A.: Phytoplankton in a changing world: cell size and elemental stoichiometry, J. Plankton Res., 32, 119–137, https://doi.org/10.1093/PLANKT/FBP098, 2010.

Giering, S. L. C., Sanders, R., Lampitt, R. S., Anderson, T. R., Tamburini, C., Boutrif, M., Zubkov, M. V, Marsay, C. M., Henson, S. A., Saw, K., Cook, K., and Mayor, D. J.: Reconciliation of the carbon budget in the ocean's twilight zone., Nature, 507, 480–483, https://doi.org/10.1038/nature13123, 2014.

Graff, J. R., Nelson, N. B., Roca-Martí, M., Romanelli, E., Kramer, S. J., Erickson, Z., Cetinic, I., Buesseler, K. O., Passow, U., Zhang, X., Benitez-Nelson, C., Bisson, K., Close, H. G., Crockford, T., Fox, J., Halewood, S., Lam, P., Roesler, C., Sweet, J., VerWey, B., Xiong, Y., and Siegel, D. A.: Reconciliation of total particulate organic carbon and nitrogen measurements determined using contrasting methods in the North Pacific Ocean as part of the NASA EXPORTS field campaign, Elem. Sci. Anthr., 11, https://doi.org/10.1525/elementa.2022.00112, 2023.

Hama, T., Miyazaki, T., Ogawa, Y., Iwakuma, T., Takahashi, M., Otsuki, A., and Ichimura, S.: Measurement of photosynthetic production of a marine phytoplankton population using a stable ^{13}C isotope, Mar. Biol., 73, 31–36, https://doi.org/10.1007/BF00396282/METRICS, 1983.

Henson, S. A., Yool, A., and Sanders, R.: Variability in efficiency of particulate organic carbon export: A model study, Global Biogeochem. Cycles, 29, 33–45, https://doi.org/10.1002/2014GB004965, 2015.

Henson, S. A., Laufkötter, C., Leung, S., Giering, S. L. C., Palevsky, H. I., and Cavan, E. L.: Uncertain response of ocean biological carbon export in a changing world, Nat. Geosci. 2022 154, 15, 248–254, https://doi.org/10.1038/s41561-022-00927-0, 2022.

Knap, A., Michaels, A., Close, A., Ducklow, H., and Dickson, A.: Protocols for the Joint Global Ocean Flux Study (JGOFS) Core Measurements. JGOFS Report Nr. 19, 1–210 pp., 1996.

Lalande, C., Moran, S. B., Wassmann, P., Grebmeier, J. M., and Cooper, L. W.: ^{234}Th-derived particulate organic carbon fluxes in the northern Barents Sea with comparison to drifting sediment trap fluxes, J. Mar. Syst., 73, 103–113, https://doi.org/10.1016/j.jmarsys.2007.09.004, 2008.

Lalande, C., Bauerfeind, E., and Nöthig, E. M.: Downward particulate organic carbon export at high temporal resolution in the eastern Fram Strait: influence of Atlantic Water on flux composition, Mar. Ecol. Prog. Ser., 440, 127–136, https://doi.org/10.3354/MEPS09385, 2011.

Lam, P. J., Ohnemus, D. C., and Auro, M. E.: Size-fractionated major particle composition and concentrations from the US GEOTRACES North Atlantic Zonal Transect, Deep Sea Res. Part II Top. Stud. Oceanogr., 116, 303–320, https://doi.org/10.1016/J.DSR2.2014.11.020, 2015.

Lam, P. J., Lee, J.-M., Heller, M. I., Mehic, S., Xiang, Y., and Bates, N. R.: Size-fractionated distributions of suspended particle concentration and major phase composition from the U.S. GEOTRACES Eastern Pacific Zonal Transect (GP16), Mar. Chem., 201, 90–107, https://doi.org/10.1016/j.marchem.2017.08.013, 2018.

Laws, E. A. and Maiti, K.: The relationship between primary production and export production in the ocean: Effects of time lags and temporal variability, Deep Sea Res. Part I Oceanogr. Res. Pap., https://doi.org/10.1016/J.DSR.2019.05.006, 2019.

Lemaitre, N.: Multi-proxy approach (Thorium-234, excess Barium) of export and remineralization fluxes of carbon and biogenic elements associated with the oceanic biological pump, Université de Bretagne Occidentale, 319 pp., 2017.

Lemaitre, N., Planchon, F., Planquette, H., Dehairs, F., Fonseca-Batista, D., Roukaerts, A., Deman, F., Tang, Y., Mariez, C., and Sarthou, G.: High variability of particulate organic carbon export along the North Atlantic GEOTRACES section GA01 as deduced from ^{234}Th fluxes, Biogeosciences, 15, 6417–6437, https://doi.org/10.5194/bg-15-6417-2018, 2018.

Maiti, K., Buesseler, K. O., Pike, S. M., Benitez-Nelson, C., Cai, P., Chen, W., Cochran, K., Dai, M., Dehairs, F., Gasser, B., Kelly, R. P., Masque, P., Miller, L. A., Miquel, J. C., Moran, S. B., Morris, P. J., Peine, F., Planchon, F., Renfro, A. A., van der Loeff, M. R., Santschi, P. H., Turnewitsch, R., Waples, J. T., and Xu, C.: Intercalibration studies of short-lived thorium-234 in the water column and marine particles, Limnol. Oceanogr. Methods, 10, 631–644, https://doi.org/10.4319/lom.2012.10.631, 2012.

Mari, X., Passow, U., Migon, C., Burd, A. B., and Legendre, L.: Transparent exopolymer particles: Effects on carbon cycling in the ocean, Prog. Oceanogr., 151, 13–37, https://doi.org/10.1016/J.POCEAN.2016.11.002, 2017.

Le Moigne, F. A. C., Poulton, A. J., Henson, S. A., Daniels, C. J., Fragoso, G. M., Mitchell, E., Richier, S., Russell, B. C., Smith, H. E. K., Tarling, G. A., Young, J. R., and Zubkov, M.: Carbon export efficiency and phytoplankton community composition in the Atlantic sector of the Arctic Ocean, J. Geophys. Res. Ocean., 120, 3896–3912, https://doi.org/10.1002/2015JC010700, 2015.

Moran, S. B., Weinstein, S. E., Edmonds, H. N., Smith, J. N., Kelly, R. P., Pilson, M. E. Q., and Harrison, W. G.: Does ^{234}Th/^{238}U disequilibrium provide an accurate record of the export flux of particulate organic carbon from the upper ocean?, Limnol. Oceanogr., 48, 1018–1029, https://doi.org/10.4319/lo.2003.48.3.1018, 2003.

Morris, P. J., Sanders, R., Turnewitsch, R., and Thomalla, S.: ^{234}Th-derived particulate organic carbon export from an island-induced phytoplankton bloom in the Southern Ocean, Deep Sea Res. Part II Top. Stud. Oceanogr., 54, 2208–2232, https://doi.org/10.1016/j.dsr2.2007.06.002, 2007.

Ohashi, K., Laurent, A., Renkl, C., Sheng, J., Fennel, K., and Oliver, E.: DalROMS-NWA12 v1.0, a coupled circulation-ice-biogeochemistry modelling system for the northwest Atlantic Ocean: Development and validation, Geosci. Model Dev., 17, 8697–8733, https://doi.org/10.5194/GMD-17-8697-2024, 2024.

https://doi.org/10.5194/egusphere-2025-3671
Preprint. Discussion started: 25 August 2025

Owens, S. A., Buesseler, K. O., and Sims, K. W. W.: Re-evaluating the ^{238}U-salinity relationship in seawater: Implications for the ^{238}U–^{234}Th disequilibrium method, Mar. Chem., 127, 31–39, https://doi.org/10.1016/j.marchem.2011.07.005, 2011.

Owens, S. A., Pike, S., and Buesseler, K. O.: Thorium-234 as a tracer of particle dynamics and upper ocean export in the Atlantic Ocean, Deep Sea Res. Part II Top. Stud. Oceanogr., 116, 42–59, https://doi.org/10.1016/j.dsr2.2014.11.010, 2015.

Parsons, T. R., Maita, Y., and Lalli, C. M.: A manual of chemical and biological methods for seawater analysis, Pergamon Press, Oxford, UK, 173 pp., https://doi.org/10.25607/OBP-1830, 1984.

Passow, U.: Transparent exopolymer particles (TEP) in aquatic environments, Prog. Oceanogr., 55, 287–333, https://doi.org/10.1016/S0079-6611(02)00138-6, 2002.

Passow, U. and Carlson, C.: The biological pump in a high CO_2 world, Mar. Ecol. Prog. Ser., 470, 249–271, https://doi.org/10.3354/meps09985, 2012.

Passow, U. and Wassmann, P.: On the trophic fate of *Phaeocystis pouchetii* (Hariot): IV. The formation of marine snow by *P. pouchetii* on JSTOR, Mar. Ecol. Prog. Ser., 104, 153–161, 1994.

Passow, U. and Weber, T.: The biological carbon pump, in: Treatise on Geochemistry (Third Edition), vol. 4, Elsevier, 333–369, https://doi.org/10.1016/B978-0-323-99762-1.00031-0, 2025.

Puigcorbé, V., Roca-Martí, M., Masqué, P., Benitez-Nelson, C., Rutgers van der Loeff, M., Bracher, A., and Moreau, S.: Latitudinal distributions of particulate carbon export across the North Western Atlantic Ocean, Deep Sea Res. Part I Oceanogr. Res. Pap., 129, 116–130, https://doi.org/10.1016/J.DSR.2017.08.016, 2017.

Puigcorbé, V., Masqué, P., and Le Moigne, F. A. C.: Global database of ratios of particulate organic carbon to thorium-234 in the ocean: improving estimates of the biological carbon pump, Earth Syst. Sci. Data, 12, 1267–1285, https://doi.org/10.5194/essd-12-1267-2020, 2020.

Reigstad, M. and Wassmann, P.: Does *Phaeocystis* spp. contribute significantly to vertical export of organic carbon?, Biogeochemistry, 83, 217–234, https://doi.org/10.1007/s10533-007-9093-3, 2007.

Reinthaler, T., Van Aken, H., Veth, C., Arístegui, J., Robinson, C., Williams, P. J. L. B., Lebaron, P., and Herndl, G. J.: Prokaryotic respiration and production in the meso- and bathypelagic realm of the eastern and western North Atlantic basin, Limnol. Oceanogr., 51, 1262–1273, https://doi.org/10.4319/LO.2006.51.3.1262, 2006.

Resplandy, L., Martin, A. P., Le Moigne, F., Martin, P., Aquilina, A., Mémery, L., Lévy, M., and Sanders, R.: How does dynamical spatial variability impact ^{234}Th-derived estimates of organic export?, Deep Sea Res. Part I Oceanogr. Res. Pap., 68, 24–45, https://doi.org/10.1016/j.dsr.2012.05.015, 2012.

Roca-Martí, M. and Puigcorbé, V.: Combined Use of Short-Lived Radionuclides (^{234}Th and ^{210}Po) as Tracers of Sinking Particles in the Ocean, Ann. Rev. Mar. Sci., 16, 551–575, https://doi.org/10.1146/annurev-marine-041923-013807, 2024.

Roca-Martí, M., Puigcorbé, V., Iversen, M. H., Rutgers van der Loeff, M. M., Klaas, C., Cheah, W., Bracher, A., and Masqué, P.: High particulate organic carbon export during the decline of a vast diatom bloom in the Atlantic sector of the Southern Ocean, Deep Sea Res. Part II Top. Stud. Oceanogr., 138, 102–115, https://doi.org/10.1016/j.dsr2.2015.12.007, 2017.

Roca-Martí, M., Benitez-Nelson, C. R., Umhau, B. P., Wyatt, A. M., Clevenger, S. J., Pike, S., Horner, T. J., Estapa, M. L., Resplandy, L., and Buesseler, K. O.: Concentrations, ratios, and sinking fluxes of major bioelements at Ocean Station Papa, Elem. Sci. Anthr., 9, https://doi.org/10.1525/elementa.2020.00166, 2021.

Roca-Martí, M., Healey, M., and Kienast, S. S.: Particulate Th-234, organic carbon, organic nitrogen and biogenic silica concentrations in size-fractionated particles in the Labrador Sea in spring 2022 [dataset], PANGAEA, https://doi.org/10.1594/PANGAEA.983961, 2025a.

Roca-Martí, M., Healey, M., and Kienast, S. S.: Total (dissolved + particulate) Th-234 and U-238 activities in seawater in the Labrador Sea in spring 2022 [dataset], PANGAEA, https://doi.org/10.1594/PANGAEA.983957, 2025b.

https://doi.org/10.5194/egusphere-2025-3671
Preprint. Discussion started: 25 August 2025

Romanelli, E., Sweet, J., Giering, S. L. C., Siegel, D. A., and Passow, U.: The importance of transparent exopolymer particles over ballast in determining both sinking and suspension of small particles during late summer in the Northeast Pacific Ocean, Elementa, 11, https://doi.org/10.1525/ELEMENTA.2022.00122/197269, 2023.

Salter, I., Lampitt, R. S., Sanders, R., Poulton, A., Kemp, A. E. S., Boorman, B., Saw, K., and Pearce, R.: Estimating carbon, silica and diatom export from a naturally fertilised phytoplankton bloom in the Southern Ocean using PELAGRA: A novel drifting sediment trap, Deep Sea Res. Part II Top. Stud. Oceanogr., 54, 2233–2259, https://doi.org/10.1016/j.dsr2.2007.06.008, 2007.

Sanders, R., Henson, S. A., Koski, M., De La Rocha, C. L., Painter, S. C., Poulton, A. J., Riley, J., Salihoglu, B., Visser, A., Yool, A., Bellerby, R., and Martin, A. P.: The Biological Carbon Pump in the North Atlantic, Prog. Oceanogr., 129, 200–218, https://doi.org/10.1016/j.pocean.2014.05.005, 2014.

Savoye, N., Benitez-Nelson, C., Burd, A. B., Cochran, J. K., Charette, M., Buesseler, K. O., Jackson, G. A., Roy-Barman, M., Schmidt, S., and Elskens, M.: ^{234}Th sorption and export models in the water column: A review, Mar. Chem., 100, 234–249, https://doi.org/10.1016/j.marchem.2005.10.014, 2006.

Savoye, N., Trull, T. W., Jacquet, S. H. M., Navez, J., and Dehairs, F.: ^{234}Th-based export fluxes during a natural iron fertilization experiment in the Southern Ocean (KEOPS), Deep Sea Res. Part II Top. Stud. Oceanogr., 55, 841–855, https://doi.org/10.1016/j.dsr2.2007.12.036, 2008.

Schoemann, V., Becquevort, S., Stefels, J., Rousseau, V., and Lancelot, C.: *Phaeocystis* blooms in the global ocean and their controlling mechanisms: a review, J. Sea Res., 53, 43–66, https://doi.org/10.1016/J.SEARES.2004.01.008, 2005.

Smith, W. O. and Trimborn, S.: *Phaeocystis*: A Global Enigma, Ann. Rev. Mar. Sci., 16, 417–441, https://doi.org/10.1146/annurev-marine-022223-025031, 2024.

Steinberg, D. K., Van Mooy, B. A. S., Buesseler, K. O., Boyd, P. W., Kobari, T., and Karl, D. M.: Bacterial vs. zooplankton control of sinking particle flux in the ocean's twilight zone, Limnol. Oceanogr., 53, 1327–1338, https://doi.org/10.4319/lo.2008.53.4.1327, 2008.

Stephens, B. M., Roca-Martí, M., Maas, A. E., Amaral, V. J., Clevenger, S., Traylor, S., Benitez-Nelson, C. R., Boyd, P. W., Buesseler, K. O., Carlson, C. A., Cassar, N., Estapa, M., Fassbender, A. J., Huang, Y., Lam, P. J., Marchal, O., Menden-Deuer, S., Paul, N. L., Santoro, A. E., Siegel, D. A., and Nicholson, D. P.: An upper-mesopelagic-zone carbon budget for the subarctic North Pacific, Biogeosciences, 22, 3301–3328, https://doi.org/10.5194/BG-22-3301-2025, 2025.

Tesdal, J. E., Ducklow, H. W., Goes, J. I., and Yashayaev, I.: Recent nutrient enrichment and high biological productivity in the Labrador Sea is tied to enhanced winter convection, Prog. Oceanogr., 206, 102848, https://doi.org/10.1016/J.POCEAN.2022.102848, 2022.

Volk, T. and Hoffert, M. I.: Ocean carbon pumps: analysis of relative strengths and efficiencies in ocean-driven atmospheric CO_2 changes, in: The Carbon Cycle and Atmospheric CO_2: Natural Variations Archean to Present, vol. 32, edited by: Sundquist, E. T. and Broecker, W. S., American Geophysical Union, Washington, D. C., 99–110, https://doi.org/10.1029/GM032, 1985.

Wiedmann, I., Ceballos-Romero, E., Villa-Alfageme, M., Renner, A. H. H., Dybwad, C., Jagt, H., Svensen, C., Assmy, P., Wiktor, J. M., Tatarek, A., Różańska-Pluta, M., and Iversen, M. H.: Arctic Observations Identify Phytoplankton Community Composition as Driver of Carbon Flux Attenuation, Geophys. Res. Lett., 47, e2020GL087465, https://doi.org/10.1029/2020GL087465, 2020.

Wollenburg, J. E., Katlein, C., Nehrke, G., Nöthig, E.-M., Matthiessen, J., Wolf- Gladrow, D. A., Nikolopoulos, A., Gázquez-Sanchez, F., Rossmann, L., Assmy, P., Babin, M., Bruyant, F., Beaulieu, M., Dybwad, C., and Peeken, I.: Ballasting by cryogenic gypsum enhances carbon export in a *Phaeocystis* under-ice bloom, Sci. Rep., 8, 7703, https://doi.org/10.1038/s41598-018-26016-0, 2018.

Yashayaev, I.: Intensification and shutdown of deep convection in the Labrador Sea were caused by changes in atmospheric and freshwater dynamics, Commun. Earth Environ., 5, https://doi.org/10.1038/S43247-024-01296-9, 2024.